FRICTION MEASUREMENTS ON LIVING HELA CELLS

Friction Measurements on Living HeLa Cells

by

MARC-ANTONI GOULET

B.Sc. (McGill) 2006

A Thesis
Submitted to the School of Graduate Studies
in Partial Fulfilment of the Requirements
for the Degree
Master of Science

McMaster University

MASTER OF SCIENCE (2008)   McMaster University
(Physics)   Hamilton, Ontario

TITLE: Friction Measurements on Living HeLa Cells

AUTHOR: Marc-Antoni Goulet

SUPERVISORS: Dr. K. Dalnoki-Veress

NUMBER OF PAGES: ix, 47

Abstract

This thesis is a study of the adhesive behaviour of HeLa cells using a novel instrument designed for measuring both the shearing and compression force applied to the cells. For these experiments a micropipette forged as a double cantilever is used to grasp and manoeuvre a cell onto a silicon or Poly-L-Lysine (PLL) coated substrate. The substrate is then moved perpendicularly with respect to the micropipette tip thereby sliding and shearing the cell across the surface. The perpendicular and parallel deflection of the cantilever enables us to directly measure the friction and normal force. A new approach for calibrating both sections of the cantilever has been developed and will also be presented in this work. As a proof of concept, the experiment is also performed with a polystyrene bead. The polystyrene bead, a simpler system, manifests some of the typical results expected from friction experiments.

Acknowledgements

A constant struggle to the bitter end, I would never have achieved this degree without the help and support of several people. First and foremost among these however, I would like to thank my supervisor Kari Dalnoki-Veress for his unwavering optimism and kindness. His amiable guidance and enthusiasm were an integral part of my persistence to continue. I could not have asked for a better supervisor. His impeccable choice of graduate students also deserves an honourable mention. Working alongside so many good people was a definite morale boost during the toughest times. Within the group, I'd like to thank Andrew for his sage advice and Adam for being such a useful resource of random information. Some other important elements of my success to note would be Joe's programming assistance and endless sarcasm, as well as Jessica's pleasant character and sense of humor. I am very grateful to Josh for keeping me active outside of the lab and on track within the lab by setting such a 'golden' example to follow. Last but certainly not least, I owe much of this thesis to Marie-Josée not only because it is primarily founded upon her hard work but also for her supportive role throughout every step of the process. Knowing that she had surmounted many of the same experimental hurdles I faced made it easier for me to keep trying.

I would like to thank Dr. Cécile Fradin for letting me use her cell culture facilities and Asmahan for training me to use them. The physics department itself deserves some mention as well. Without such a large amount of good people to keep me sane and entertained I certainly would not have made it this far. Although my time here was brief, I managed to make a lot of good friends that I hope to see again.

Outside of the department, I would like to mention my Aikido sensei J. Cho and Megumi Harada for giving me a reason to wake up so damn early in the morning. Although far away, my family back in Montreal were always interested in my progress and having something positive to tell them was another motivating factor behind my work. Finally, I would also like to give thanks to my best friend Zhenia for her endless support and compassion during these past two years.

MARC-ANTONI

Contents

List of Figures

Chapter 1

Introduction

The evolutionary jump from single-celled organisms to multicellular organisms would not have been possible without the phenomenon of biological adhesion. The non-specific and isotropic nature of colloidal interactions are insufficient to permit a micron sized cell to 'choose' its environment. Fortunately, most living cells are equipped with specific adhesion mechanisms with which they can bond preferentially to other cells in order to form a multicellular organism such as ourselves. This attachment and detachment mechanism is also partially responsible for their ability to 'crawl' on and adhere to a substrate that is favorable to their survival.

Understanding this process is vital for biomedical applications such as implants. Typically our cells must be able to bind to the foreign material being implanted into the body in order for the implant to be successful. In some cases such as the design of an artificial joint, the friction or adhesion between the foreign and natural tissue needs to be minimized to reduce wear; attaining the very low friction coefficient between our natural joint tissues being the goal [1]. Rather than looking at the macroscopic properties of tissues, this study investigates friction and adhesion at the microscopic level of the single cancer cell. Adhesion plays an important role in the metastacization cycle of cancer development. It is during this stage that a cluster or single cancer cell will be detached from a tumor and migrate to another region of the body, adhering to different tissue and forming a new tumor.

The ultimate goal of this research is to study the dynamics of cell adhesion by looking at the cells sliding during our friction experiments. A brief review of the theory behind cellular adhesion is first presented followed by an overview of the relevant aspects of tribology. Some previous studies pertaining to adhesion are then introduced and a detailed description of our experimental procedure is given in the subsequent chapter. We then present some of our results and conclude with some ideas about the direction this project may take in the future.

Chapter 2

Review

2.1 Cell adhesion

When observing cells free floating in medium, they appear as spherical objects much like simple lipid bilayer vesicles. The cells used for this project are HeLa cancer cells, fibroblasts which range from 10-20 μm in size. At this scale and below, the surface area becomes more important than the bulk in the sense that the interfacial forces between the cell and other objects become dominant [2]. Objects in this size range are termed colloids and the sum of all interfacial forces which govern their behavior with respect to each other is known as the colloidal interaction. The competing forces involved in this interaction determines whether the colloids will adhere to each other and form an aggregate or not. In addition to the colloidal interaction, living cells also have more specific adhesion mechanisms which will be discussed later.

2.1.1 Van der Waals interaction

In the absence of any external forces, two neutral colloids in vaccuum will tend to adhere to each other if brought sufficiently close together. This phenomenon can be explained by the van der Waals interaction. The van der Waals force is due to the attraction between the dipoles in each colloid. If we consider only two neutral atoms first, there can be an attraction between their permanent electric dipole moments (the Keesom force), the attraction between the permanent moment of one atom and the induced dipole in the other (the Debye force), and also the attraction between the fluctuating dipoles of each atom due their electronic movements (the London force) [3]. The potential energy of all of these effects combined is often written in the form,

$$V(r) = -Cr^{-6};$$

(2.1)

where C is the coefficient for the simplified atom-atom potential and r is the distance between the two atoms. Although the van der Waals force is weak compared to thermal motion at the atomic

level, the interaction of two extended surfaces composed of many atoms can amount to a very large attractive potential. When dealing with the attraction between a roughly spherical cell and a planar substrate as in our experiments, the van der Waals potential will take the form given by Israelachvili [4],

$$V(r) = \frac{-(\pi^2 C \rho_1 \rho_2 R)}{6r}; \tag{2.2}$$

where ρ_i is the density of the atoms being considered in each object, R is the radius of the cell and r is the distance from the cell to the substrate. For a non-uniform object such as a cell the coefficient C will depend on the atomic composition of the membrane. Integrating this energy with respect to the distance we can obtain the van der Waals force,

$$F(r) = \frac{-(\pi^2 C \rho_1 \rho_2 R)}{3r^2}. \tag{2.3}$$

This force remains dominant at relatively long range depending on the geometries being considered. For our case we can expect to see an effect at distances on the order of 10 nm [4].

2.1.2   Osmotic repulsion

The interface responsible for most of the colloidal interaction of living cells is their outer lipid bilayer membrane and its constituents. As shown in Fig. 2.1, the lipid bilayer is composed primarily of two sheets of phospholipid molecules which are stacked tail-to-tail such that the hydrophilic polar head groups are facing the aqueous environment inside and outside the cell. Most of these phospholipids are capped by a charged section such as choline, ethanolamine, serine, etc., in addition to the charged phosphate group.
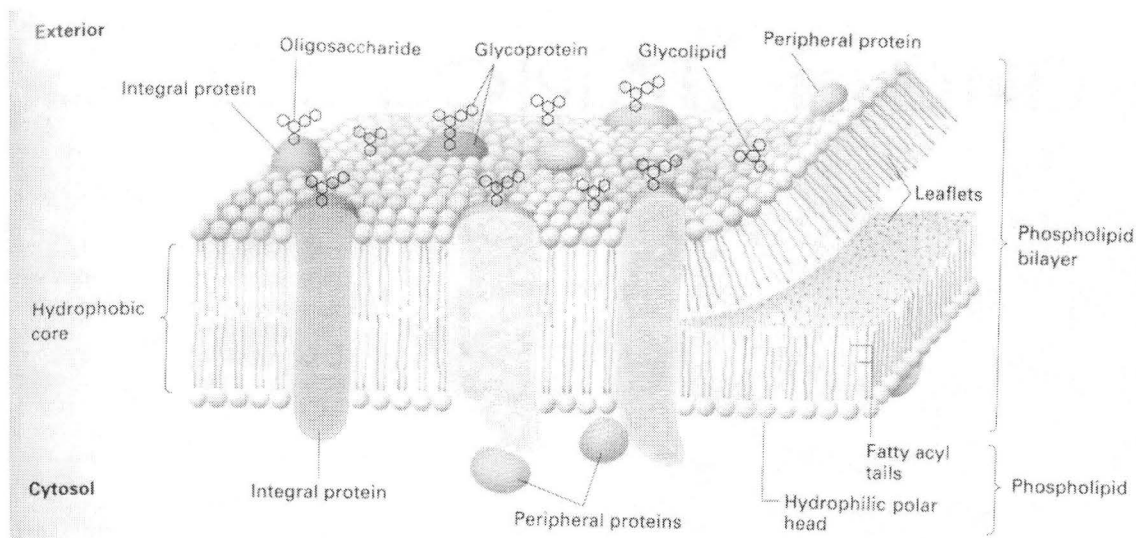
Figure 2.1: Schematic of cell membrane. [5]

It is natural to assume that the net charge of the membrane would create an electrostatic repulsion effect between two similar cells opposing the van der Waals interaction. In an electrolyte solution such as the phosphate buffered saline(PBS) solution used in our experiments however, the dissolved ions tend to screen the charges of cells and substrates typically reducing the electrostatic interaction at certain ranges. The effect is similar to the cancellation of the electric field within a conductor by the rearrangement of the electrons. Whatever electrostatic repulsion remains is not in fact due to the surface or dissolved ionic charge directly but to the osmotic pressure created by the higher concentration of ions between both surfaces.

2.1.3   Entropic repulsion

The presence of other large molecules on the outer layer of the lipid bilayer further complicates the colloidal interaction. From Fig. 2.1, we can see several polysaccharides attached to both phospholipids and membrane proteins. This layer of relatively stiff polysaccharide chains is known as the glycocalyx and forms a physical barrier often preventing the membrane from coming close

enough to other surfaces for the van der Waals force to have an appreciable effect [6]. Longer and more flexible polymers may also exist on the membrane. Depending on the density of these attached polymers, entropy will favor certain steric configurations. At high densities they will tend to form polymer brushes that extend out into the extracellular matrix, with an effective volume that mimics the effect of the polysaccharide chains [3].

Another type of repulsive entropic effect is due to the random thermal fluctuations of the membrane itself, causing the membrane to undulate and therefore resist compression. An example from Boal illustrates that a 1 μm^2 patch of lipid bilayer with a bending modulus of 20 $k_b T$ can have a mean displacement of 20 nm at room temperature [3]. Such large local deformations prevent the cell from coming into intimate contact with another surface.

2.1.4 Depletion interaction

If the solution which contains the cells also contains other large polymers such as proteins there will be an added attractive osmotic force. Depending on the size of the polymers in solution, there will be a layer surrounding the cells or any other surface in which no polymers will be found. It is essentially the entropic repulsion or steric hindrance of the dissolved polymers. This excluded volume is known as the depletion zone and is related to the radius of gyration R_g of the polymer. When any two surfaces become sufficiently close, their depletion zones will overlap creating a region of low polymer concentration. Since no polymers can enter this region, there is an osmotic effect which tries to eliminate the region by pushing the two surfaces closer together.

2.1.5 Biological adhesion

Unfortunately, all of the colloidal interactions discussed up to this point are insufficient to fully characterize the adhesion of living cells. For the most part, the glycocalyx (roughly 10 nanometers in thickness) and membrane undulations make long range attraction unlikely. Moreover, the membrane is dependent on the rearrangement of the interior cytoskeleton which often leads to folds in the membrane. For this reason cells typically do not spontaneously adhere to surfaces through ideal uniform colloidal interactions (wetting or spreading on the surface) [6]. Cells tend to adhere by forming discrete short range molecular bonds rather than by continuous interfacial forces. Intimate contact with a surface is achieved through cell motility or mechanical impingement in order to smooth out the membrane. The molecular bonds or bridges formed are focal in nature, atomic in distance and often irregularly distributed due to their dependence on the concentration of adhesive glycoproteins in that particular area of the membrane or surface. The bonds themselves however can be very strong, from 5 $k_b T$ for certain protein-ligand pairs up to 35 $k_b T$ for a single biotin-avidin bond [7,8]. As opposed to the colloidal interaction, this type of process leads to irreversible adhesion where the spontaneous adhesion energy, W_a, can be much less than the detachment energy, W_f. For certain bonds, the force required to detach the cell can be higher than the structural integrity of

the membrane itself, leading to extrusion of the adhesive protein [9,10]. It has been shown however, that any constant force will eventually break a biological noncovalent adhesion bond given enough time [11]. Similarly, another study by Merkel [12] demonstrates that the rupture force for the biotin-streptavidin bond increases as the rate of the applied force is increased.

A complete understanding of the adhesion between cells requires an intimate knowledge of which receptors and ligands are participating in the process. Unfortunately, creating a full compendium of the multitude of these 'adhesins' is an enormous undertaking. Biologists so far have managed to classify the known mammalian adhesion molecules into four large groups: integrins, selectins, cadherins and the immunoglobulin superfamily [6].

Without knowing more about the chemistry of our particular HeLa cell membranes it is imposible to determine which adhesion mechanism we are studying. From a purely physical point of view however there are some general measurements which apply to all types adhesion, namely the magnitude and timescale of the rupture force. Over the past few decades, some progress has been made in understanding the mechanics of cell adhesion for specific systems using these types of measurements. These experiments are described in the next section.

2.2   Previous adhesion experiments

Studying a complex object such as a cell can be a daunting task. A common approach to studying complex systems is to try and minimize the complexity by considering only a few elements of the system at a time. Another approach is to determine the response of the entire system to a controlled parameter. Both of these approaches have been applied to the problem of measuring the adhesion forces of living cells. In either case the challenge is to apply a known force while varying other parameters such as the loading rate, the duration of attachment, the substrate, etc.

2.2.1   Micropipette aspiration techniques

Some of the earliest cellular adhesion measurements were performed by Evans *et al.* with the help of micropipette aspiration experiments. By applying a known suction pressure to a red blood cell at the end of a micropipette they could control its membrane tension. Controlling the tension of one blood cell, he could contact another cell held at the end of another pipette. Building on his earlier work with the deformation of the red blood cell, he could then use the cell itself as the force transducer [13]. This experiment was later modified to use vesicles bearing low amounts of receptors and ligands. The tension of vesicles could be controlled such that force measurements in the piconewton range became possible [9]. This technique was further improved by chemically coupling microscopic latex beads to the vesicles and adding piezoelectric pipette control [14].

2.2.2 Flow chamber techniques

Another way of introducing a calibrated force into a biological experiment is to use the viscous force of the medium moving with respect to the cell. A series of recent experiments by Décavé et al. use a lateral or radial flow chamber to apply a specific force to an array of incubated and adhered cells [15–17]. The force applied to each cell is dependent on its size and location within the chamber. These studies support their model for a peeling type of detachment mechanism which is based on receptor diffusion. According to the 'lipid raft' model of the cell membrane, elements such as phospholipids and proteins are free to move within the lipid bilayer but not outside of it, essentially behaving like a two dimensional liquid crystal [18]. In an attempt to recreate a real world immune response scenario, an experiment led by Goetz looks into the probabilistic nature of bond formation between leukocytes and the endothelium. This technique involves using a flow chamber to push neutrophil cells along a substrate covered with endothelial tissue. The round cells roll along the tissue until an adhesive bond is formed and the cell stops momentarily [19]. By varying the shear stress applied to the cells they observe different binding rates related to the probability of receptor attachment.

2.2.3 Cantilever techniques

Using cantilevers to apply calibrated forces to objects is an old technique that has found widespread usage within the physical sciences. Studies by Yamamoto et al. use an L-shaped cantilever to apply a lateral force to the side of a cell adhered to a substrate [20, 21]. They use this method to measure the detachment force of the cell while visualizing the contact area through an optical microscope. By coating the substrate with proteins such as collagen and fibronectin, or using polystyrene or glass surfaces, they compare the interaction strength between the cells and these materials.

With a resolution of around 10 pN, some groups have also used atomic force microcscopes to perform single molecule adhesion measurements. The idea to use this technique to study individual ligand-receptor interactions was pioneered by Florin et al. in 1994 [22]. Coating the tip of an AFM with biotinylated albumin and approaching this tip to streptavidin-coated beads they could measure the detachment force when the tip was pulled away. By repeating this process over and over again they could detect a quantization in the force measurements indicating the strength of a single ligand-receptor pair.

As it turns out, our group is not the first to use specially forged micropipettes as cantilevers. This technique was independently used by Francis et al. for one study in 1987 but was never developed further [23]. Similarly to the work done by my predecesor Marie-Josée Colbert, this study uses a bent micropipette to manoeuvre a cell onto a substrate and measure the force involved during detachment. Whereas their experiment focuses exclusively on the magnitude of the detachment force, the experiments in this thesis are concerned with the dynamics of this detachment process.

2.3   Friction

As the epitome of non-conservative forces, the presence of friction during any mechanical process necessarily leads to kinetic energy being converted to unusable thermal energy. Due to the growing importance of mechanization in our society, this loss of energy through friction has generated a renewed interest in the field of tribology which has led to a greater understanding and appreciation of the intricacies of friction. A basic model for friction is first presented followed by some of the refinements to the theory which apply to our experiment.

2.3.1   Basic friction model

Following the treatment of friction from a first year textbook [24], we begin by considering the force of kinetic friction which opposes the motion of a solid object sliding on a surface. In this model presented in eq. 2.4 , the force of friction F_k is proportional to the normal or loading force N and depends only on this variable. The constant of proportionality μ_k is defined by the interaction between the surface and the object,

$$F_k = \mu_k N. \tag{2.4}$$

Another type of friction called static friction is defined as the force which opposes the commencement of motion of an object on a surface. This is a passive force since by definition the object is not moving and hence the force of static friction F_s is equal and opposite to the applied force. This relation holds until the applied force is greater than the maximum force of static friction and the object begins to move. The relation is defined as,

$$F_s \leq \mu_s N; \tag{2.5}$$

where and μ_s is the constant of proportionality for the two surfaces being considered. The maximum force of static friction is given by the equality of equation 2.5.

2.3.2   Typical tribology experiments

The essential elements for performing friction experiments is to apply a known normal force and measure the resulting friction force. The surface forces apparatus conceived for measuring the van der Waals forces between two surfaces is often utilized for tribological measurements of macroscopic objects [4]. This instrument consists of two crossed cylinders whose distance from each other can be controlled down to angstrom resolution. Different materials such as mica can be placed on the contact areas between the cylinders. A double spring system can measure the shearing and loading force. Lubricating layers can be introduced and studied at various thicknesses by applying different loading forces to the cylinders. Another type of instrument used to study friction is the friction force microscope (FFM). Utilizing the same cantilever principle as the atomic force microscope (AFM), where the bending of a calibrated cantilever provides the known force, this

apparatus measures the torsion or lateral motion of the cantilever as opposed to the vertical motion. The FFM was designed for measuring friction at the atomic scale [25]. Although our experiment is not designed for this type of resolution, the cantilever principle is the same.

2.3.3   Sliding, stick-slip and chaotic motion

Once an object begins to slide with respect to a surface, we can consider three possible outcomes for the subsequent motion.

1. The object can continue to slide smoothly along the surface according to the basic model of kinetic friction.

2. The object can stick and slip chaotically.

3. The object can stick and slip periodically.

Typically, the sliding regime occurs when the spring constant of the cantilever is very high (very stiff) or the velocity is above a certain threshold. As the velocity is decreased below this threshold the chaotic regime begins. Decreasing the velocity further causes a stable periodic stick-slip phenomenon [25]. The transition between periodic, chaotic and smooth motion can be thought of like any other phase transition. For instance a study by Drummond and Isaelachvili demonstrates a continuous transition between these regimes for an ultrathin lubricating film of the branched hydrocarbon squalane between two mica sheets [26]. This is in contrast to other studies with smaller linear hydrocarbon lubricants which have discontinuous first order transitions [27].

2.3.4   Soft materials

The idea of stick-slip motion denotes a very abrupt transition. This is to be expected for harder materials that have little compliance. When studying the stick-slip motion of soft materials such as gel, rubber or living cells we can anticipate a smoothing effect at lower velocities due to the slower relaxation time of these materials. This mechanical relaxation is the subject of several studies by Baumberger *et al.* dealing with 'self-healing slip pulses' of a gel moving on a glass surface [28,29]. The results from one of these experiments show a time dependence for the maximum force of static friction. They explain this by noting that longer contact time allows the soft material to relax and form more intimate contact with the surface.

2.3.5   Surface lubrication

Given the fact that our experiments take place in an aqueous environment we need to consider the possibility that surface lubrication could have a dominant effect. The basic idea behind hydrodynamic lubrication is that a sufficiently thick layer of liquid remains trapped between the two surfaces such that the friction force is dependent on the laminar flow of the liquid rather than the interaction of the surfaces. An interesting consequence of this is that a viscous liquid will be more easily trapped between two surfaces and therefore lead to hydrodynamic lubrication more easily but it will also be more resistant to laminar flow. Starting with the Navier-Stokes and continuity equations for an incompressible liquid it is possible to solve for the friction force due to this resistance to laminar flow. The function and its derivation are contained in the book by Persson but will not be displayed here [25]. The most important thing is that the resultant friction force depends on viscosity, velocity, normal force, and is typically much smaller than for the unlubricated or boundary lubricated (film thickness of only a few molecular layers) surfaces.

Chapter 3

Experimental Procedure

The first generation of this experiment consisted of measuring only the shearing force applied to a cell with the use of a straight micropipette acting as a cantilever. A full characterization of the friction between two surfaces however requires knowledge of the pressure or normal force between these two surfaces as well as the shearing or friction force. In our current experiment we measure both the friction and normal force simultaneously by forging a very flexible micropipette with a 90° angle to act as a double cantilever. During an experiment, a cell being held at the end of this micropipette can be compressed and sheared by the substrate, thereby deflecting each section of the cantilever. After calibration of each section, we can obtain the normal and friction force by analyzing their deflection in the images recorded.

As a method of verifying the viability of our technique, we perform the same type of experiments with a polystyrene bead. This simplified experiment allows us to make sure that the general trends we see such as stick-slip motion are not artifacts. Moreover, it enables us to compare a soft gel-like cell with a harder material of the same size and shape.
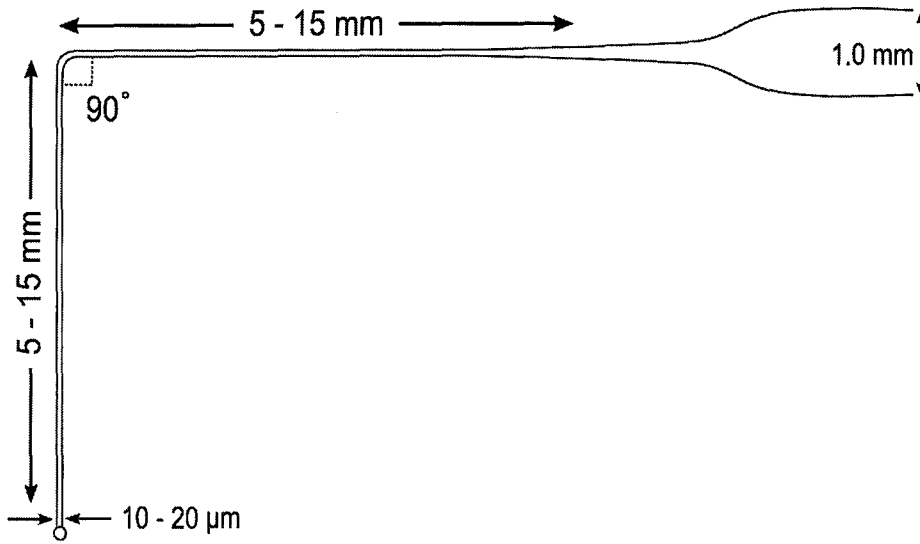
Figure 3.1: Diagram of micropipette cantilever.

3.1   Micropipette fabrication

We use glass capillary tubes (Kimble Glass Inc., model 464885) which have an outer diameter of 1.0 mm as a starting material to make our force transducing micropipettes. These glass capillaries are pulled to an outer diameter of 10-20 μm with a horizontal pipette puller (Narishige model PN-30). Occasionally, the tip of the micropipette will be open, but when this does not occur we can cut the micropipette open with a homemade microforge. For this microforge we use a three-dimensional micromanipulator (Narishige, model M-152) to position the micropipette onto a platinum wire (0.508 mm diameter, $\tilde{0}.4$ Ω). The wire is heated with a current from a DC power supply (Xantrex regulated DC power supply HPD 30-10). As the voltage is increased the wire expands and eventually melts the micropipette which wets the platinum wire. With the help of an optical microscope (Meiji Techno, model SKT 28209), the molten glass is wrapped around the wire to ensure good adhesion. The power supply is then switched off completely creating an abrupt cooling and contraction of the wire. As the wire pulls back, the micropipette solidifies and breaks at the junction point. This process typically creates a micropipette tip with a flat opening which is perpendicular to the shaft. Using the wire at a lower voltage, the micropipette can be heated just enough to forge it into a 90° angle around the midpoint of the shaft. In the end, we obtain a double cantilever as shown schematically in Fig. 3.1.

3.2   Sample preparation

3.2.1   Cell culture

As previously mentioned, the cells we use in this experiment are HeLa cancer cells from the P5-P10 generation. These cells are cultured in 5 ml of α-MeM media to which we add 10% fetal bovine serum, 1% antibiotic Penicyllin and 0.1% fungizone. Once a cell line is started, the cancer cells divide roughly every 24 hours for as long as there is fresh media in the petri dish and they are incubated at 37°C with 95% relative humidity and 5% CO_2. Every few days, the cells must be split into new dishes in order to accomodate the growth of new generations. The old media is removed, the dish washed with 2.5 ml of 1% PBS saline solution, and 500 μl of 1% trypsin is added to detach the cells. Once the cells are detached, 2 ml of new media is added. Several 300-500 μl portions of this solution can be extracted and deposited into new dishes containing 5 ml of fresh media to start a new colony.

For the purposes of an experiment, the cells are extracted when they are in suspension during this last splitting phase. Roughly 100 μl of the cells and media are diluted with 3 ml of 1% PBS. This solution can then be inserted into the open chamber on the microscope. The cells can survive in this environment for several hours.

3.2.2   Polystyrene beads

For the simpler version of our experiment, we use 20 μm polystyrene beads (Polysciences, Inc. Polybead R). A drop of these beads is inserted into the chamber which has already been filled with pure Millipore filtered water.

3.2.3   Subtrate

The substrate we use is made from three inch polished Si(001) wafers which are cleaved into 1X9 mm sections just small enough to fit inside the open chamber on the microscope. These pieces are then individually cleaned by placing them on a hot plate and spraying them with supercritical CO_2. They are then treated in a UV/ozone chamber (Bioforce Laboratory) for 30-40 minutes to remove residual organic impurities. When studying specific adhesion, the clean pieces of silicon are immersed in a 1% Poly-L-Lysine (PLL) solution overnight. Just before the experiment they are rinsed to remove excess PLL.

When conducting an experiment, the substrate is tied to the long arm of a custom made holder with the help of paraffin strips. The holder is mounted on the micromanipulator and the substrate is inserted into the chamber (see Fig. 3.2).

3.3   Experimental set-up

In order to visualize the micron sized cell and micropipette, the entire experiment is performed on an Olympus IX71 inverted microscope. An open chamber is constructed from glass coverslips spaced apart by $\sim$ 2 mm and mounted on the microscope stage. The cells (or beads), their media, the substrate and the micropipette are inserted into the chamber as shown in Fig. 3.2. The capillary force is sufficient to constrain the fluid between the coverslips.
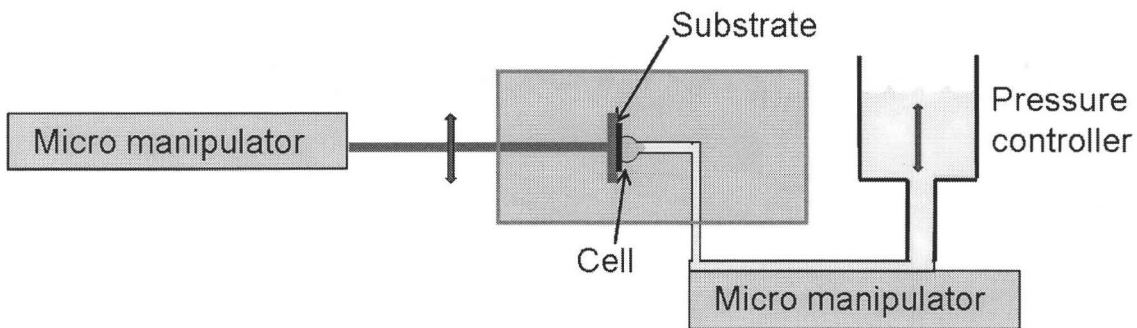

Figure 3.2: Schematic of experimental setup.

A water column with an adjustable height is conected to the micropipette and used as a manometer to provide the negative pressure necessary for grabbing and holding onto the cells. In the case of the harder beads, a syringe is used to provide the much larger suction required. We can then manoeuvre the pipette and cell into position next to the substrate with the help of a micromanipulator (EXFO PCS 5000). The substrate is mounted on a separate micromanipulator controlled by computer. Once everything is in place, the substrate is moved into the cell, compressing it, and deflecting the normal force section of the micropipette backwards with a certain normal force. The substrate is then moved parallel to the contact area according to the Labview program parameters, deflecting the shearing force section of the cantilever as in Fig. 3.3. A mirror image of the cell and pipette is visible in Fig. 3.3 because the reflective silicon substrate is tilted slightly downwards into the microscope objective. The tilted substrate creates a clearer image of the contact area since only a small part of the substrate is in focus at any given time. The mirror image also helps to align the substrate perpendicular to the pipette.

These brightfield images are captured using a CCD camera (Q-Imaging Retiga 2000R) and recorded with the Labview program. The entire experimental set-up, excluding the computer, rests on an anti-vibration table (Halcyonics, MOD-1) to reduce the noise.
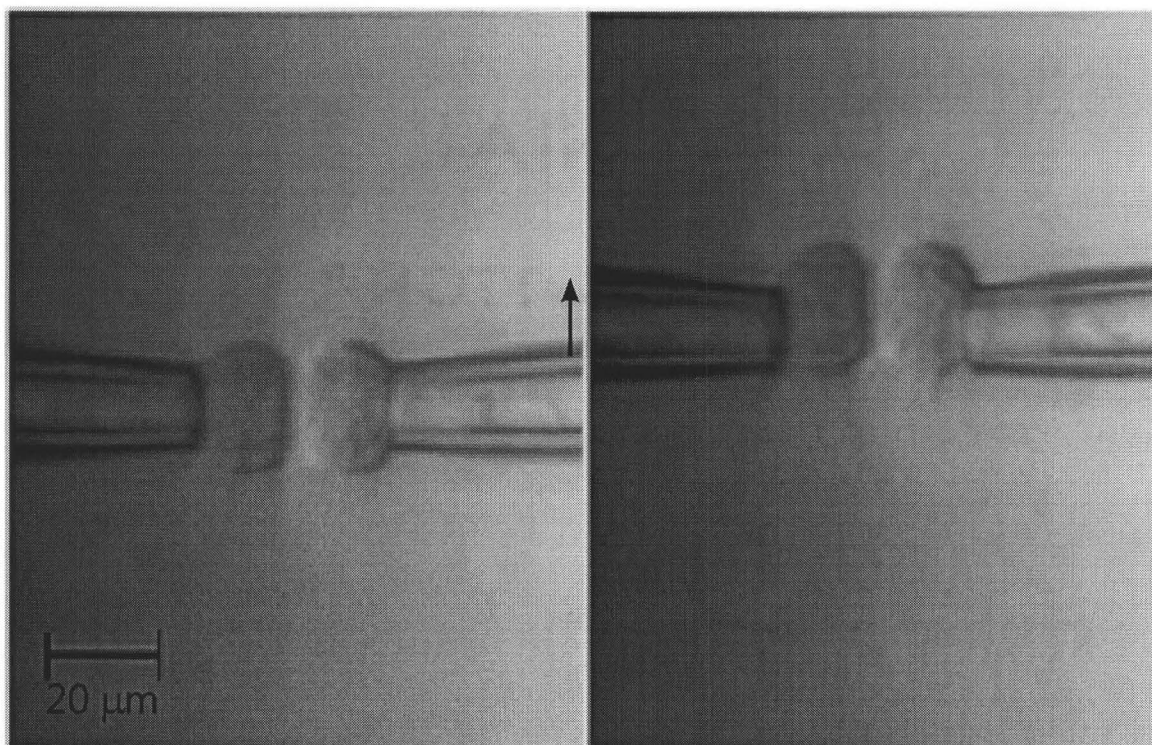
Figure 3.3: Images of friction experiment on HeLa cell. The image on the right shows the cell being sheared and the micropipette being deflected upwards. Note the deformation of the cell in response to shearing.

3.4 Labview Program

The Labview program written for this experiment is based on the previous incarnation designed by Marie-Josée Colbert for her project. The snapshot in Fig. 3.4 shows the control panel of the program.
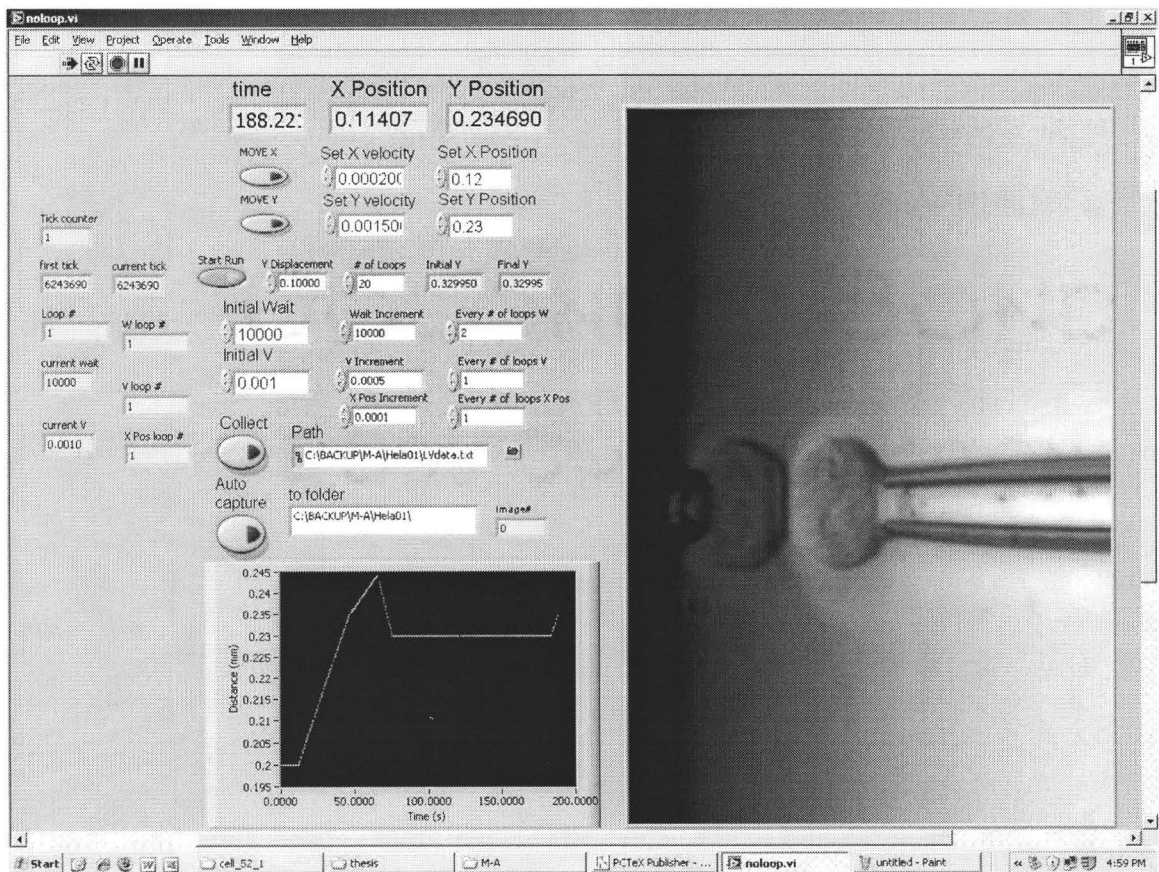

Figure 3.4: Screenshot of Labview program.

When the program is running, it cycles through an iteration and updates the time, position, and the video portion of the panel about every 300-500 ms depending on the size of the image. The program can be used manually, with the top section of the panel to move the substrate into the cell (x-axis), or in the shearing directions (y-axis). The speeds accessible with either actuator can range from 0.1 - 300 μm/s. The program can also be automated to move in a given number of sections while changing 3 possible parameters for each section: the wait time between sections, the speed of substrate motion, and the x position of the substrate which is the normal force applied to the cell.

As an example, we can take the sample experiment in the picture (Fig. 3.4). Once the substrate has been manually moved into the cell. The 'Start run' button is pressed at which point the following happens:

1. The subtrate waits an initial time of 10000 ms.

2. The substrate moves at 1.0 μm/s.

3. When it has finished moving 100 μm, it stops and waits 10000 ms.

4. While waiting, the substrate moves further into the cell by 0.1 μm.

5. When the wait time is over, the substrate begins to move at 1.5 μm/s.

6. After finishing the 2nd section, the substrate waits 20000 ms and moves further into the cell by 0.1 μm.

7. After the 20000 ms, the substrate begins to move at 2.0 μm/s.

this process continues for 20 sections of 100 μm, changing the wait time every 2 sections, whereas the velocity and normal force change every section.

The time and position of the substrate throughout the experiment can be recorded to a text file for future analysis and pictures can be recorded into a folder at the program cycling rate or slower if necessary. A small graph at the bottom left of the control panel indicates the y position of the substrate with respect to time for the whole time the program is running.

3.5 Image analysis

For the 1-dimensional case of tracking the micropipette deflection of our earlier friction experiments, I used the cross-correlation program written for Matlab by Adam Raegan. This cross-correlation technique compares the intensity profile of a line for any given image and compares it to the intensity profile of the same line for the first image. The lines are shifted with respect to each other in every possible permutation and multiplied together, the maximum multiplicative value corresponding to the most likely shift in position of the elements in the line (ie: the new micropipette position).

Unfortunately, this simple multiplication doesn't work well for situations in which the background elements may have a stronger influence than the tracked object. For the 2-dimensional case where we wish to know the movement of the micropipette tip both parallel and perpendicular to the substrate, this is indeed the case. Several variations on the original cross-correlation program were attempted, but none resolved the issue. A new method based on least squares estimation was developed instead.
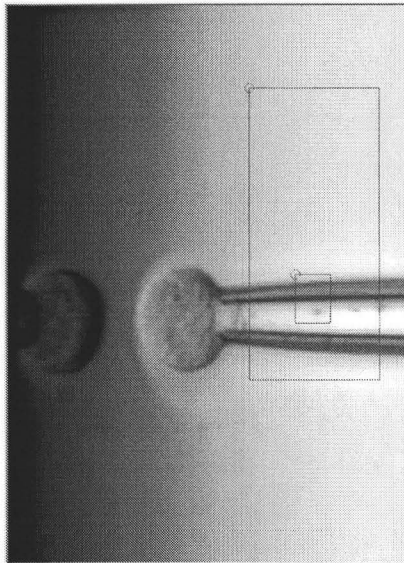
Figure 3.5: Screenshot of region of interest selection during matlab analysis.

As in the first case, the grayscale image is manipulated as a matrix of intensity values whose elements correspond to the pixels of the image. A rectangular section of the picture corresponding to the object being tracked is selected graphically by the user, called matrix A. Another larger section is selected as the possible range of motion throughout the experiment as in Fig. 3.5, this larger is called matrix ROI.

For all subsequent images, the program finds the most likely position for the object within the range of motion rectangle. It does this by comparing the matrix A from the first image, to every possible submatrix of ROI of the same size in the image being analyzed. Starting in the top left corner of the ROI in the new image, the program selects a matrix B of the same size as A. It then computes the sum of the square of the difference between the two matrices, as in eqn. 3.1,

$$\widehat{LSE} = \sum_i \sum_j (A_{ij} - B_{ij})^2. \tag{3.1}$$

This is essentially the same as a linear regression analysis for the slope of a graph. If the top left corner of the ROI of the new image happens to correspond to the location of the object (matrix A), then we expect the estimator $\widehat{LSE}$, the sum, to be small. The program rasters across the entire ROI pixel by pixel, selecting a matrix B and computing the sum for each posssible location. The minimum of all the computed sums gives the most likely pixel position for the object. We can multiply all the sum values by -1, turning the minimum into a peak. We can expect the pixels around this peak to be gaussian due to noise. Fitting a 2-D gaussian to this peak and its adjacent

points provides subpixel resolution.

This entire process is repeated for each subsequent image and thereby the position of the object in each image is determined relative to the first image. The position can then be plotted versus image number to show the motion of the pipette.

3.6 Calibration

In order to calibrate each section of the cantilever we need to apply a known force and measure the deflection it causes. We developed a method of using the weight of a pure water droplet to bend the pipette downwards. For calibration purposes we connect the micropipette to a syringe filled with water. A syringe pump pushes water out at a slow and constant rate. The expelled water forms a droplet at the tip of the micropipette which grows in size until it falls off. The cantilever section being calibrated is positioned perpendicular to gravity by eye using the micromanipulator. Visualizing the vertical deflection of the micropipette on a horizontal tabletop microscope requires placing a mirror at a 45° angle to the tabletop. Illuminating the micropipette from the side, the light reflects off the mirror down into the microscope. For calibrating the friction force cantilever, we obtain images of the type shown in Fig. 3.6: For the normal force, the tip is angled downward
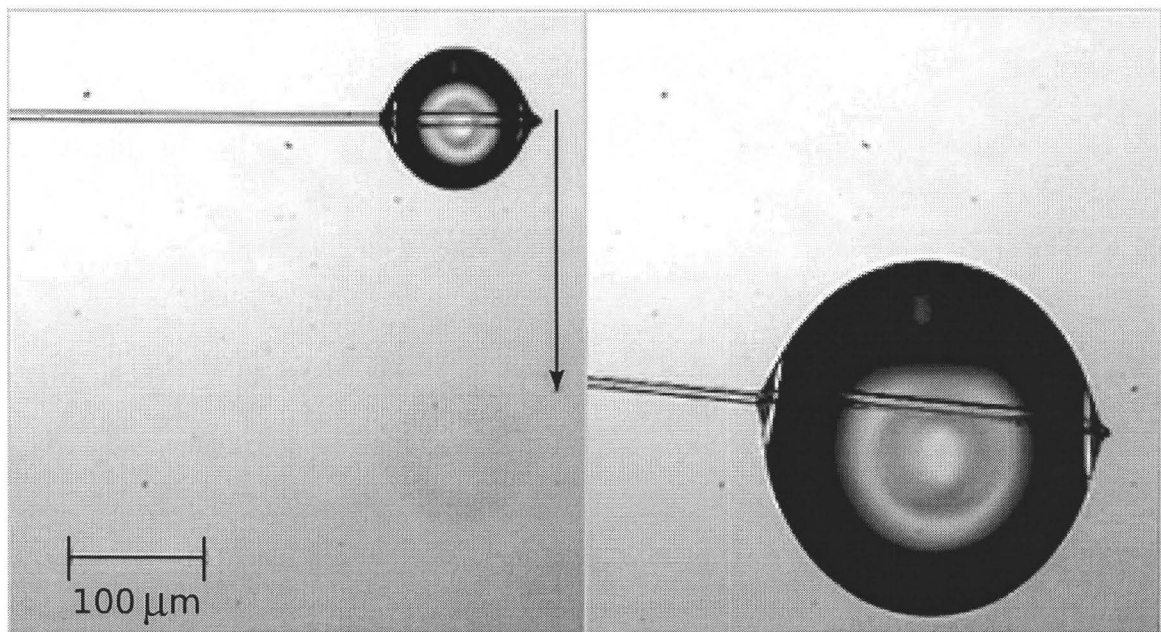

Figure 3.6: Images of water droplet bending friction force portion of micropipette downwards.

such that the normal force section is horizontal. Although this section is not in the field of view, by tracking the tip of the micropipette we can still infer its vertical displacement as in Fig. 3.7.
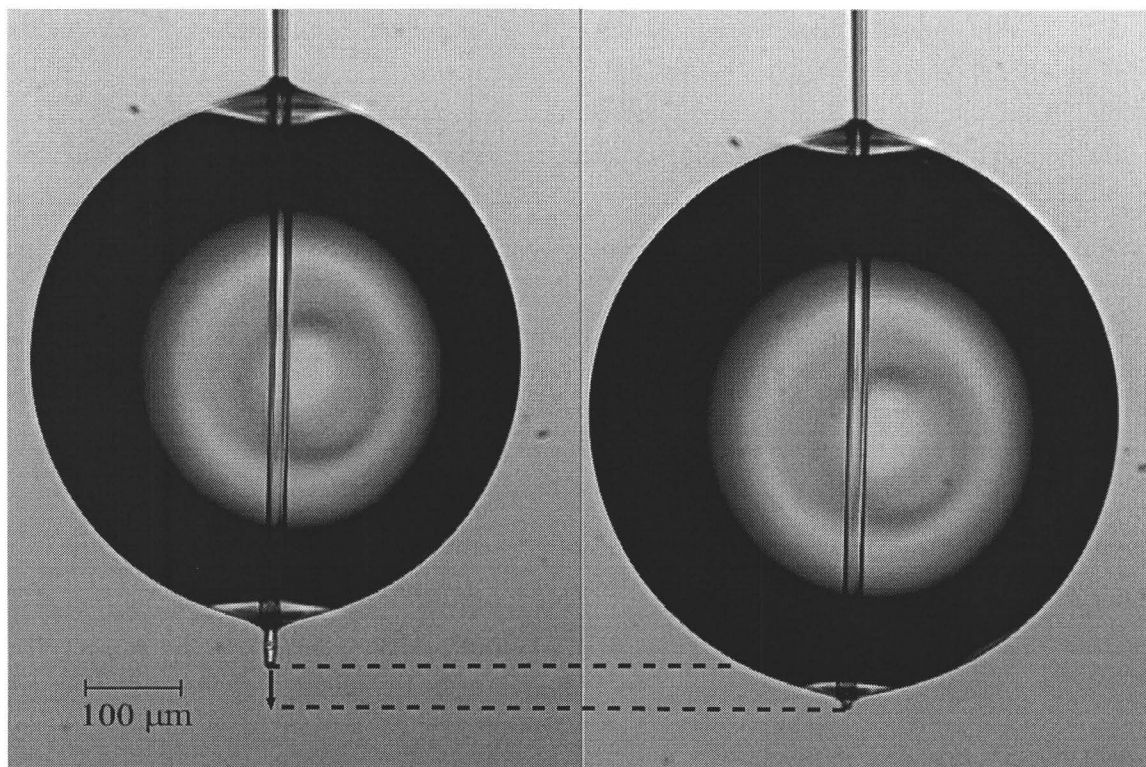
Figure 3.7: Images of water droplet bending normal force portion of micropipette downwards.

The growth of the water droplet is tracked with the help of the National Instruments Vision Assistant 8.0 program. The script written for this program selects a threshold intensity value for each image, removes all smaller particles, smooths out the remaining shapes and finds the dimensions of the rectangle encompassing the remaining droplet sized object. These rectangular dimensions are used to fit an ellipse to the droplet from which we can calculate the volume. With the known density of water the weight of the water droplet can be plotted as a function of the displacement of the micropipette. The graph of this data fits a linear slope which reveals the spring constant of the cantilever as shown in Fig. 3.8. The cantilever in this example has a spring constant of 0.68 ± 0.03 nN/μm but cantilevers ranging from 0.5-1000 nN/μm have also been forged.
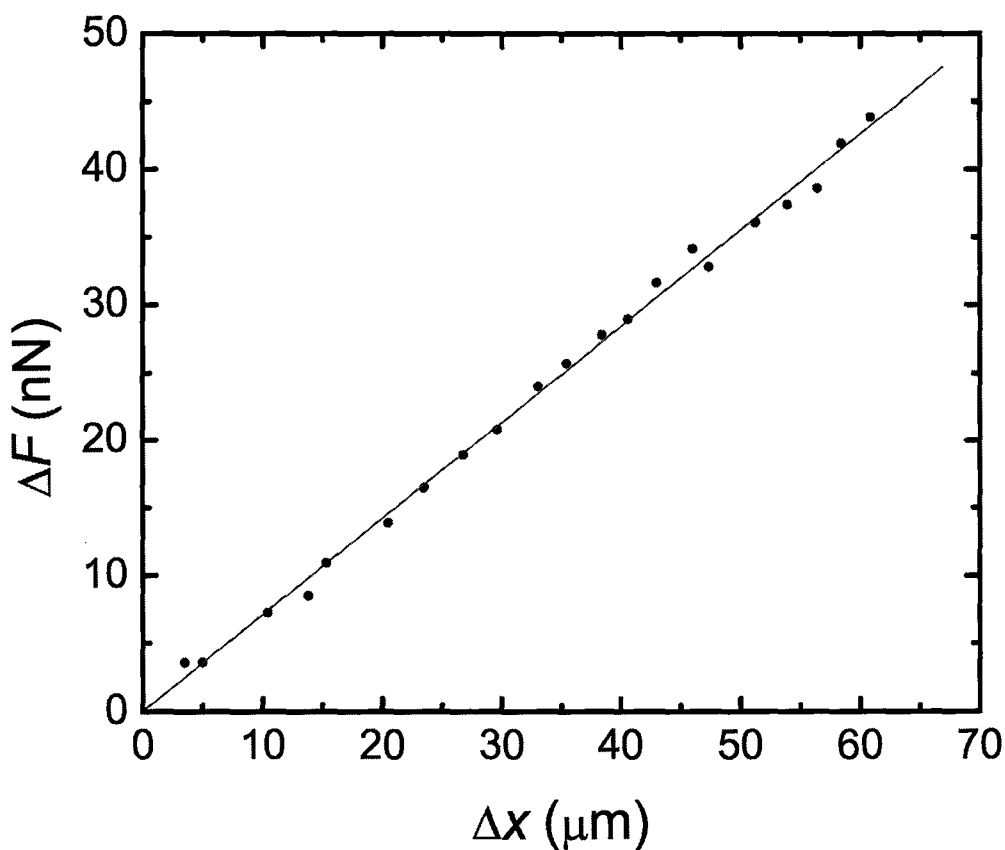

Figure 3.8: Force from calibrating droplet as a function of the micropipette displacement.

Chapter 4

Results

The majority of the experiments conducted for this project were done using living HeLa cells. Unfortunately, the variability between cells made it very difficult to collect data with which we could compare the physical characteristics of each cell in any quantitatively meaningful way. Moreover, the migration and development of an individual living cell over the duration of each experiment added to the complexity of the data and irreproducibility of the results. For this reason it became increasingly necessary to attempt the same measurements with a more standardized object in order to verify the reproducibility of the technique itself. These measurements on polystyrene beads are presented first as a validation of our micropipette technique.

4.1   Friction on polystyrene beads

As a good example of a typical friction measurement, the graph presented in Fig. 4.1 shows two sections of stick-slip motion. When the substrate begins to move around $t=125$ s, the polystyrene bead sticks to the silicon surface and moves in the same direction and the force increases. Once a certain maximum force of static friction is attained, the bead slips with respect to the substrate and the pipette moves back towards its equilibrium position. Before reaching equilibrium, the bead sticks again, repeating the same pattern over and over again until the substrate stops around $t=225$ s. After waiting 10 seconds, the substrate begins to move again in the same direction. During the next 100 seconds the same pattern is observed with a slightly higher maximum force of static friction and larger amplitude of stick-slip motion. The slope of the graph during each 'stick' cycle stays relatively constant, indicating that the substrate is always moving at the same velocity. The regularity of the stick-slip motion also indicates that we are indeed in the periodic regime of friction.
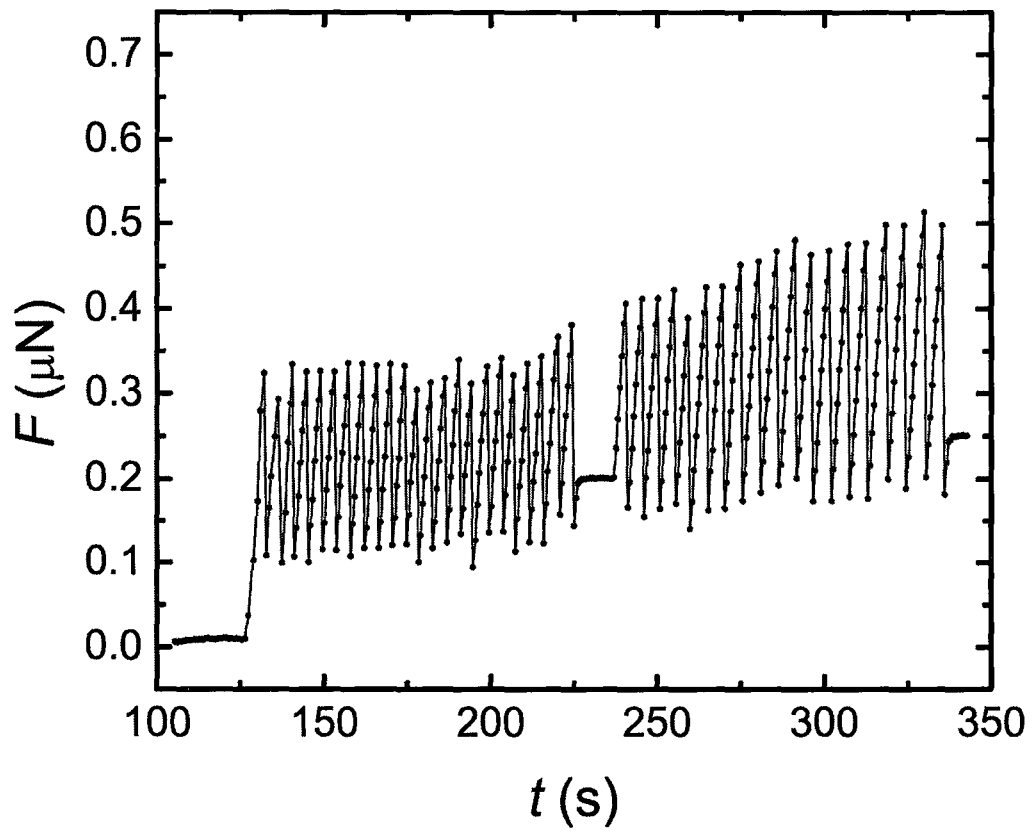
Figure 4.1: Close-up of friction force as a function of time for a polystyrene bead on silicon.

The graph shown in Fig. 4.1 shows the first 350 seconds of the experiment shown in Fig. 4.2:
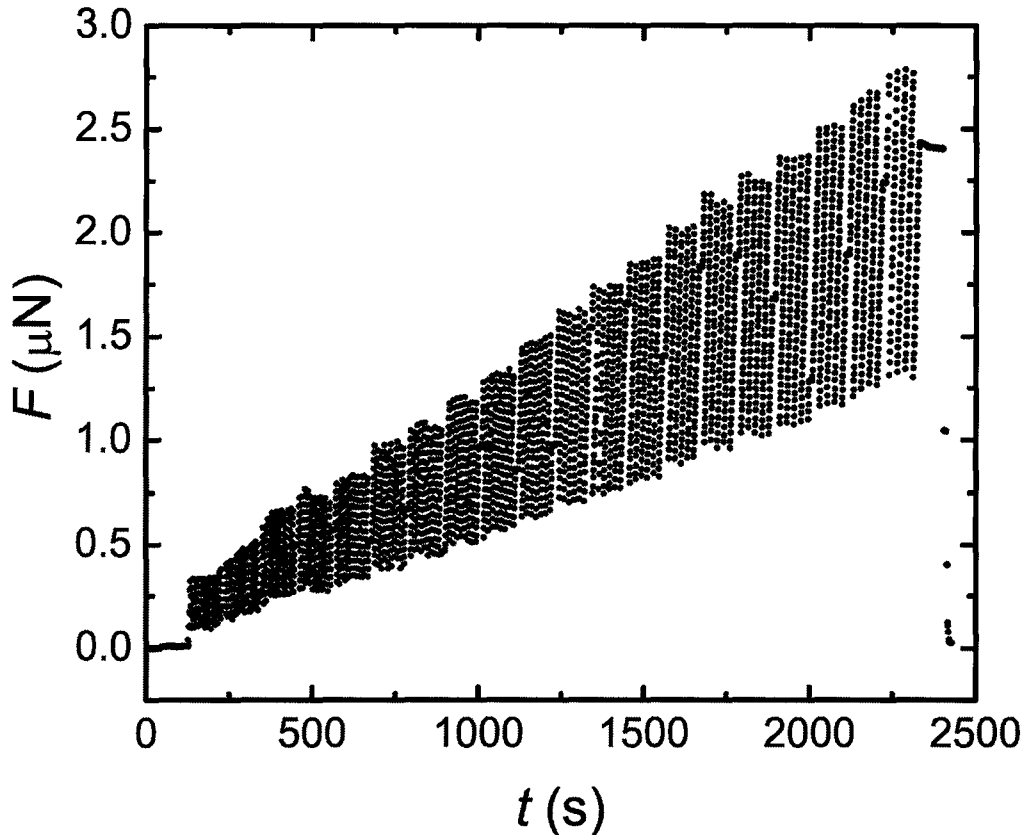

Figure 4.2: Friction force as a function of time for a polystyrene bead on silicon.

The data shown in Fig. 4.2 is composed of 20 sections of stick-slip motion with a 10 second wait time for which the substrate is motionless in the shearing direction. Each section in the graph is a result of 100 μm of substrate motion at 1 μm/s (which is indeed equivalent to the slope during each stick event). The most noticeable feature from this graph is the linearly increasing amplitude of the stick-slip force as well as the maximum force of static friction from section to section. The reason for this increase is because during each 10 second wait interval, the substrate is moved further into the bead by roughly 0.2 μm thereby increasing the normal force. At the end of the experiment, the substrate is retracted completely and the micropipette relaxes quickly to its equilibrium position.

Looking at the graph of the normal force for this same experiment in Fig. 4.3 justifies the above reasoning. In this figure we can easily see that the normal force is indeed increasing linearly from section to section verifying the relationship between normal and friction force. One issue to note is the variation of the normal force within each section. Even though the substrate motion is entirely perpendicular to the pipette during each section, the normal force varies in a stick-slip manner equivalent to the friction force. This phenomenon can be explained with geometrical arguments about the pipette or the axis of images and is primarily due to the large strength of friction leading to severe pipette deflection. The large strength of friction also causes the bead to roll out of the pipette slightly, creating a larger distance between the substrate and pipette tip and thereby pushing the pipette backwards. Performing the same experiments with a stiffer friction cantilever and higher suction pressure would minimize this effect. In any case, these graphs demonstrate the quality of data which is achievable with our instrument.
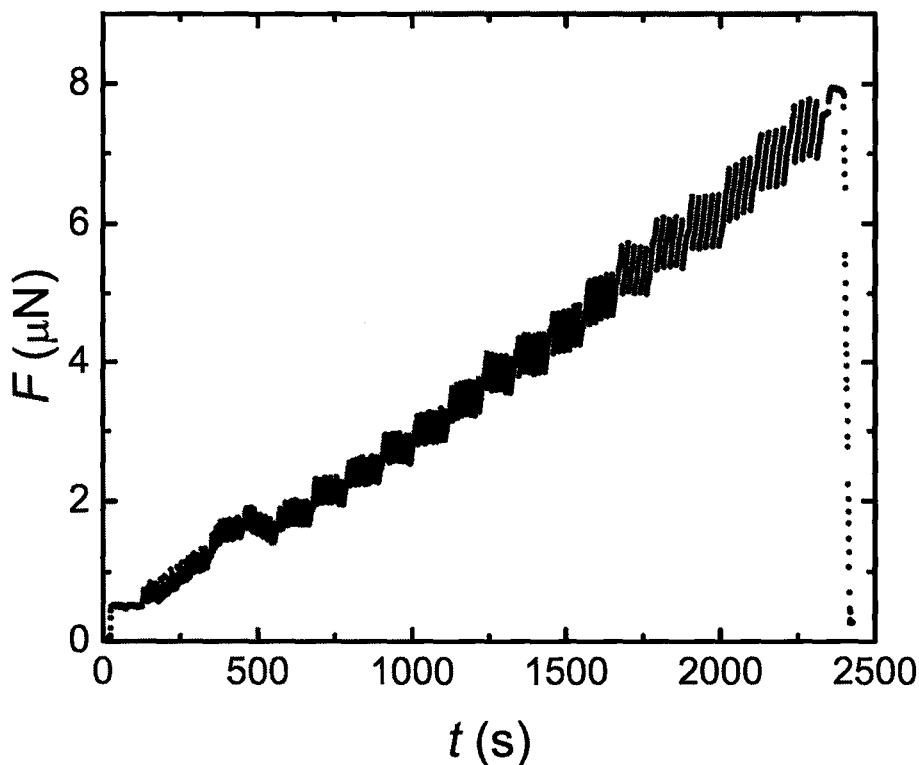

Figure 4.3: Normal force as a function of time for a polystyrene bead on silicon.

Before moving on to our experiments with cells, other experiments involving beads are presented which have verified more of the principles previously discussed. In the top half of Fig. 4.4 we see a very noisy but relatively constant sliding friction force dotted with a few sharp peaks indicating a 'stick' and a few 'dips' to be discussed later. In this experiment, 10 sections of 100 μm are traversed by the substrate moving at 1 μm/s. Between each section the substrate waits 10 seconds and moves into the cell by 0.5 μm. Again this increase in normal force is obvious from the bottom part of Fig. 4.4 but seems to have little or no effect on the friction force. The silicon substrate in this case however was coated in PLL. It has been shown by Raviv *et al.* that with two charged hydrophilic surfaces, as in this case, friction can be greatly reduced due to both entropic repulsion and hydrodynamic lubrication [30]. Although this interesting phenomenon warrants further study it is only included here to illustrate a few points. The most important detail to consider is the drastic change in behaviour between the PLL and pure silicon case. This provides clear evidence that we are indeed coating the substrate with PLL, a fact that was called into question by the large variation in cell behaviour. Another aspect which becomes apparent is the added complexity when using PLL rather than pure silicon. We can expect the increased noise and reduced friction force to add to the difficulty of performing these same measurements on living cells.
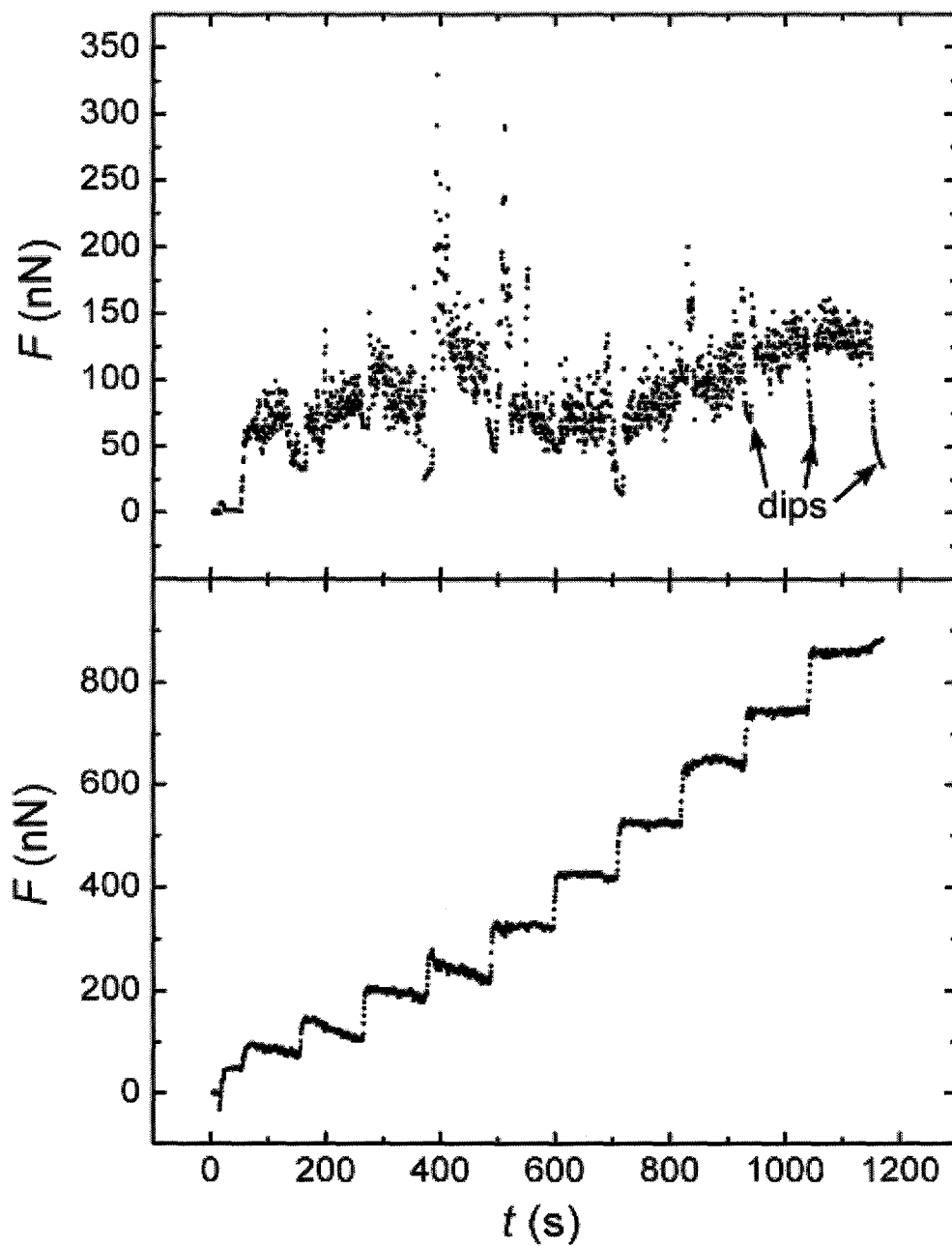
Figure 4.4: Friction force (top) and normal force (bottom) as a function of time for a polystyrene bead on silicon coated with PLL.

By changing the parameters of the previous experiment we can take a more detailed look at the 'dips' shown by arrows in Fig. 4.4. Once again we consider the friction force of a bead on a PLL coated substrate moving at 1 μm/s for 200 μm per section. In this case however we are increasing the wait time between section by 10 seconds. For the first section the substrate waits 60 seconds before moving whereas the substrate waits for 110 seconds after the last section. This longer wait time allows us to clearly see the relaxation 'dip' of the pipette back towards its equilibrium position in Fig. 4.5. This feature which was lacking in the pure silicon case of Fig. 4.1 is further evidence of the compliant nature of the PLL layer. This graph was also displayed here to demonstrate one of the greatest experimental difficulties. The curved increasing trend in friction force throughout the experiment is unfortunately not due to a controlled increase in normal force. The substrate position parallel to the pipette was maintained for the entire experiment. This curved trend is due to thermal expansion of the apparatus which has been minimized but not entirely eliminated in its latest incarnation.
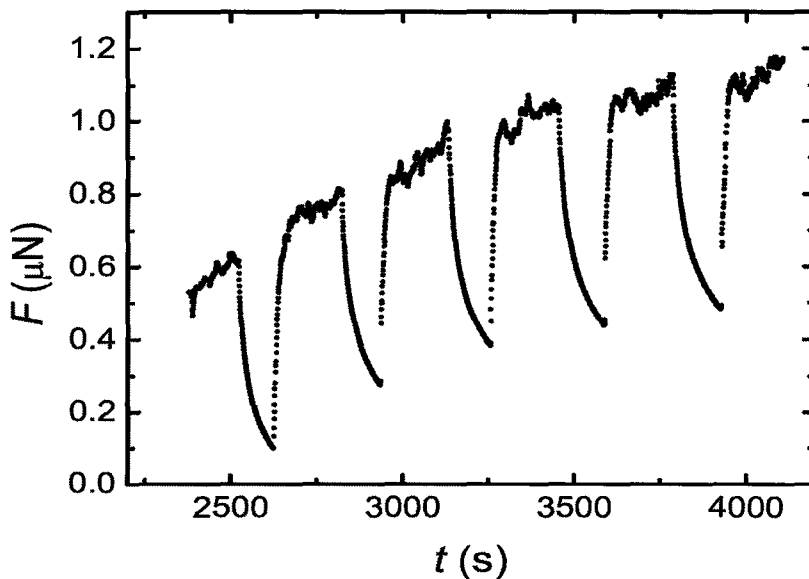

Figure 4.5: Friction force as a function of time graph showing relaxation of a polystyrene bead into PLL layer.

4.2   Friction on HeLa cells

Based on other friction studies [28, 29] of soft materials, we expect to see behavior similar to that depicted in Fig. 4.6. As the substrate begins to move, it shears the cell and drags the micropipette along to a point of maximum static friction (A). At a maximum deflection the force on the cell is large enough to overcome adhesion and the cell begins to slide with respect to the substrate, relaxing to the steady state configuration corresponding to its kinetic friction value (B). When the substrate motion stops, the cell relaxes further to another steady state value of static friction (C). This process can then be repeated in the opposite direction (D).
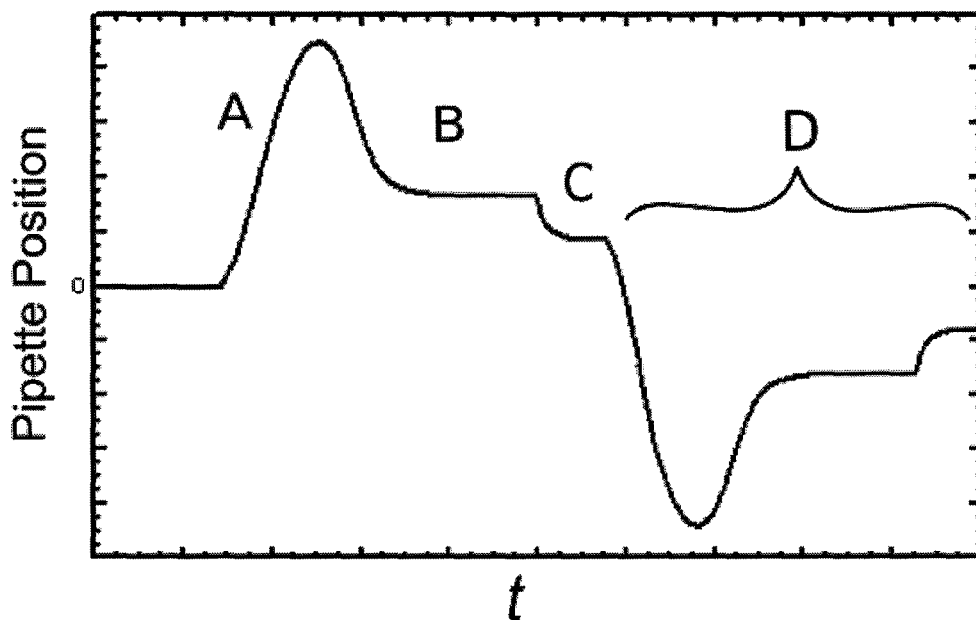

Figure 4.6: Schematic of pipette motion during friction experiment.

The friction forces seen in the polystyrene bead experiments ranged from 0.05 - 3 μN. As previously mentioned however, living cells do not typically adhere to surfaces through non-specific van der Waals forces and as such we can expect the area of contact, and therefore the shearing force, to be comparatively small. For a clean and atomically smooth surface such as silicon this is indeed what we observe, but with the help of more sensitive cantilevers we can measure forces down to a fraction of a nanonewton. As a good example of this, Fig. 4.7 shows the friction force of a living HeLa cell on a substrate moving 200 μm at 0.5 μm/s. After an initial contact time of 60 seconds, the substrate begins its motion and drags the cell and pipette with it. Once the maximum force of static friction is reached around 12 nN, the cell begins sliding and the pipette relaxes to a steady state kinetic friction value. The rounded edge of the static friction peak is due to the cell being sheared and rolling out slightly from the pipette, relaxing as a soft material typically does. There is also an absence of significant peaks with a slope equivalent to the velocity of the substrate during the sliding motion, indicating that there are no major stick events.

For this same experiment, the normal force is also recorded and shown in Fig. 4.7. During the initial 60 seconds of contact, the normal force is increasing because the substrate is moving into the cell. Since the cell is compressed between the pipette and substrate and therefore ellipsoidal in shape, it tends to push the pipette further back as it rolls out of the pipette. Once the cell begins to slide with respect to the substrate, the normal force relaxes to a steady state value.

We can take an average of both the friction and normal forces during the steady state interval, giving $F_k = 6.4 \pm 0.2$ nN and $N = 4.1 \pm 0.2$ nN respectively. Using eq. 2.4, we can then easily determine the coefficient of kinetic friction for this particular cell on silicon, namely $\mu_k = 1.6 \pm 0.1$, which is in the range of a rubber on a dry surface [31]. The data presented here gives a good idea of the quality that is achievable in our measurements. The lack of drift or significant noise makes it clear that micropipettes can be used as a viable force transducer. Simple friction measurements such as this are not the primary goal of this research. Besides the possiblity of analyzing the relaxation curves, studying the dynamics of cell adhesion requires varying certain time related parameters which will be discussed in the next section.
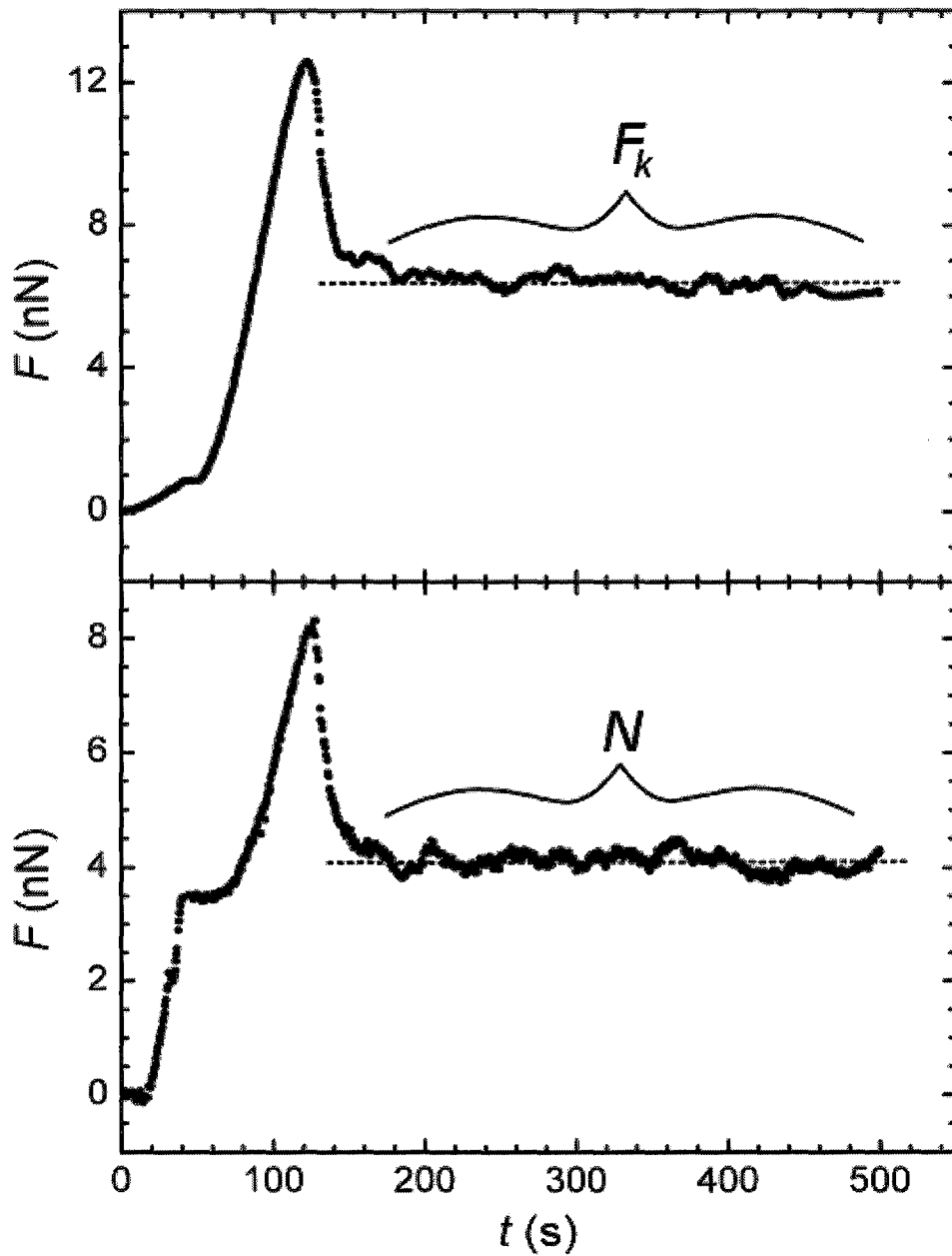
Figure 4.7: Friction force (top) and normal force (bottom) as a function of time for HeLa cell on silicon.

4.3   Specific vs. Non-specific adhesion

A simple way of studying the time dependence of adhesion is to vary the time the cell remains in contact with the same area of the substrate. The example given in Fig. 4.8 is for a cell on a silicon substrate moving 200 μm at 1 μm/s. Contrary to the bead case, this experiment and the following ones use a cyclic substrate motion as in typical friction experiments. Instead of moving in one direction in several sections, the substrate in this case moves back and forth over the same 200 μm. For this reason, the pipette gets deflected in both directions and gives both positive and negative forces. In this case, the cell is initially in contact with the substrate for 300 seconds. This wait time is increased by 60 seconds every time the substrate starts a new cycle. For this experiment, the strength of adhesion represented by the maximum force of static friction F_s, is notably constant regardless of the wait time.
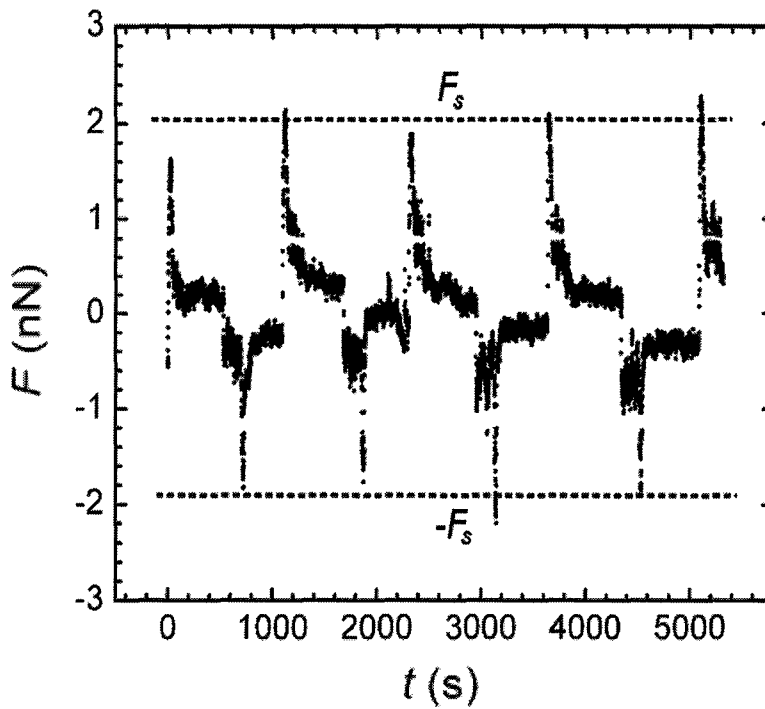

Figure 4.8: Friction force as a function of time for a HeLa cell on silicon with increasing wait times.

According to a paper by Mazia *et al.* [32], PLL adsorbs quite readily to a variety of surfaces and promotes cell adhesion and spreading. PLL is a positively charged polymer chain or protein whose cationic sites combine with the anionic sites on cell membranes. In their paper they claim that the cells will 'attach themselves as soon as they settle'. This behaviour has not generally been observed in our experiments, though in several instances relatively stronger adhesion has been noticed on PLL rather than silicon given a sufficient amount of contact time. Moreover, the detachment of cells from PLL is often accompanied by deformation of the membrane at discrete attachment sites indicating a specific adhesion process is taking place.

With this in mind, we can perform the same experiment for which we increase the wait time on a substrate coated with PLL. The data in Fig. 4.9 is for a HeLa cell on such a substrate moving back and forth for 200 μm at 2 μm/s. In this case, the initial wait time is 11 seconds and increases by 1 second every loop. Even for such a small increase in wait time, the adhesion force increases appreciably.
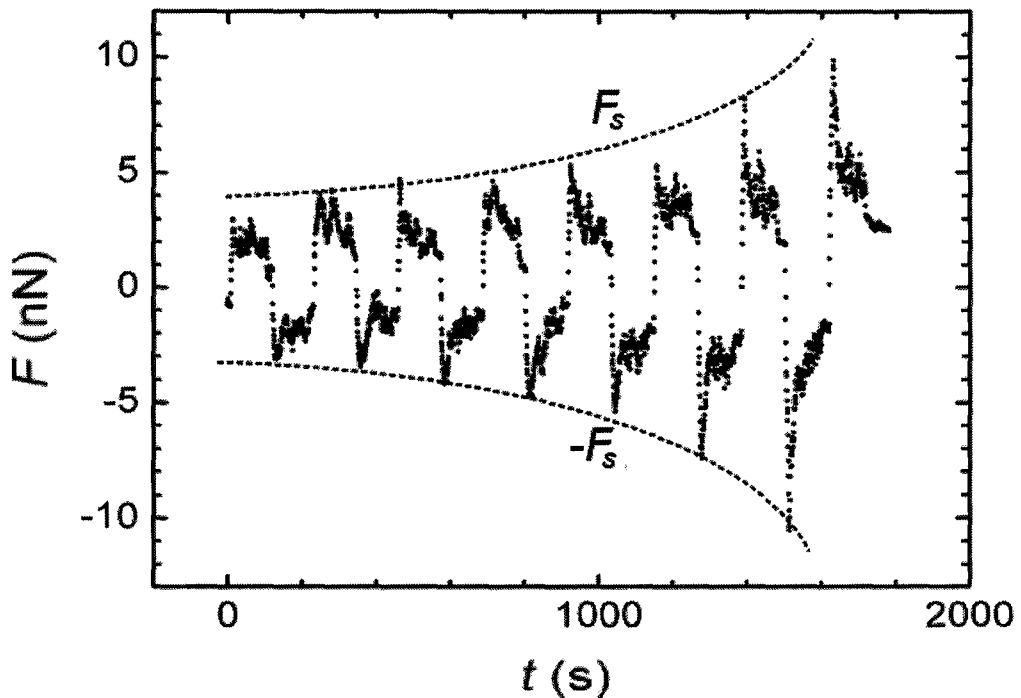

Figure 4.9: Friction force as a function of time for a HeLa cell on PLL with increasing wait times.

The contrast between Fig. 4.8 and Fig. 4.9 seems to indicate that given a substrate that is favorable to specific adhesion, cells will tend to adhere more and more strongly as time progresses. At first glance, this is to be expected given the probabilistic nature of biological adhesion rather than the direct van der Waals forces. At this stage, more experiments need to be performed to properly support this claim. The most confounding factor to eliminate is the variability between cells. An identical experiment needs to be performed using the same cell on both substrates. This was attempted by coating only half of the substrate in PLL but has not yet been successful. Also it is important to use the same parameters for each substrate. The much larger wait times used for silicon could have hidden a possible time dependence at faster timescales. Indeed, if we accept the argument by Baumberger *et al.* [28] previously mentioned, then we can expect a slight time dependence for the static friction peak simply due to relaxation of cell closer to the substrate. The main reason why these issues remain is that the friction of a cell on silicon is often so small that it is drowned out by noise and so Fig. 4.8 is difficult to reproduce. The trend seen in Fig. 4.9 for PLL however has been seen quite often and some of these datasets are presented in the appendix.

4.4   Stick-slip motion

Looking back to the polystyrene bead case in Fig. 4.1, it is obvious that the bead is fully sticking to the substrate because the slope during each stick event is equivalent to the velocity of the substrate. Finding true stick-slip behaviour like this while using a living cell is a direct way of probing the dynamics of adhesion. The original idea behind this project was to study this stick-slip behaviour while varying the velocity of the substrate in an attempt to find the transition between sliding, chaotic stick-slip and possibly even periodic stick-slip motion. The variability between cells made this goal very difficult to achieve. In most cases, the hardest challenge was to find a cell which would adhere strongly enough during motion so that we could differentiate between a proper stick event and the noise. Although the cells typically interact very weakly with pure silicon, Fig. 4.10 shows a clear example of seemingly chaotic stick-slip motion due to several peaks having a slope equal to the velocity of the substrate. The stick-slip motion shown in Fig. 4.10 is consistent with a friction measurement in the chaotic regime and does not necessarily indicate the presence of specific adhesion. The cell had an initial contact of 10 seconds after which the substrate moved one section of 200 μm at 0.2 μm/s and then retracted. The slower velocity of the substrate is likely a necessary condition for stick-slip but was not sufficient to induce this behaviour in other attempted cases.
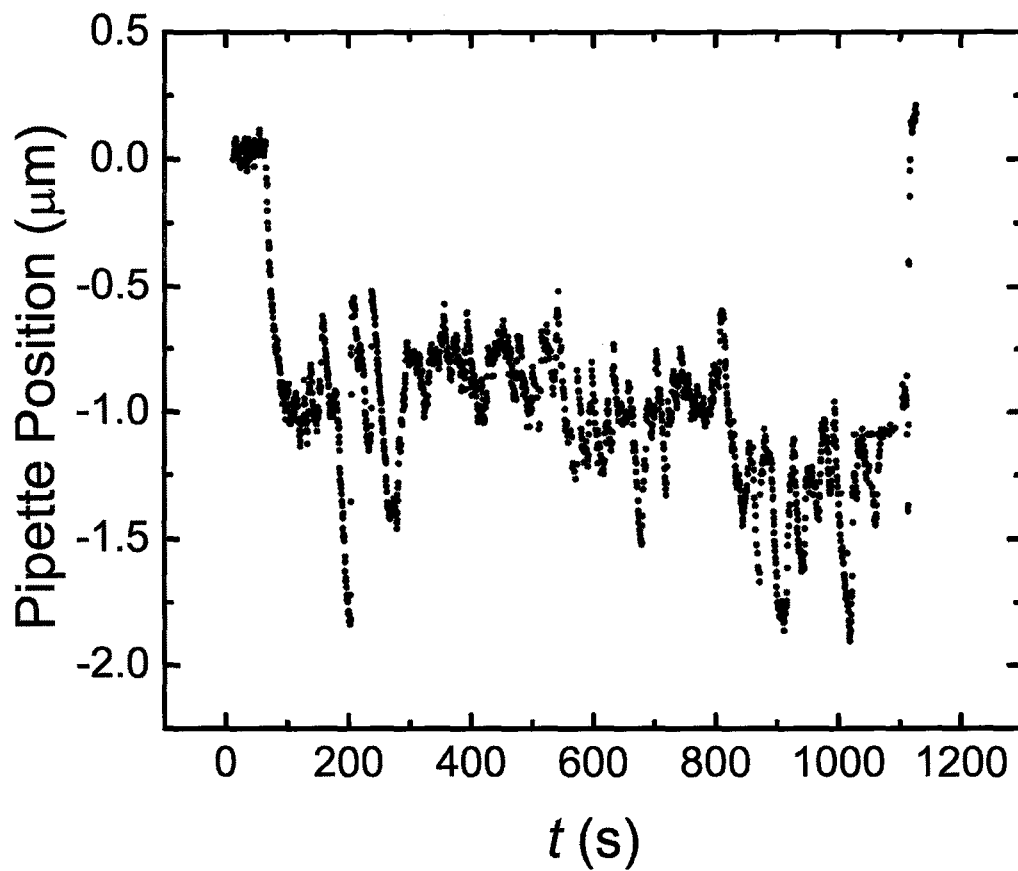
Figure 4.10: Vertical pipette position (friction force) as a function of time graph showing stick-slip motion of a HeLa cell on silicon.

Choosing a substrate which favors strong specific adhesion was our approach for maximizing the probability of biological stick-slip motion. This was the impetus for using PLL in the first place. One of the very first trials provided the most exciting results. As opposed to the typical silicon case pictured in Fig. 3.3, the cell adheres very strongly and becomes far more sheared during this experiment as depicted in Fig. 4.11.
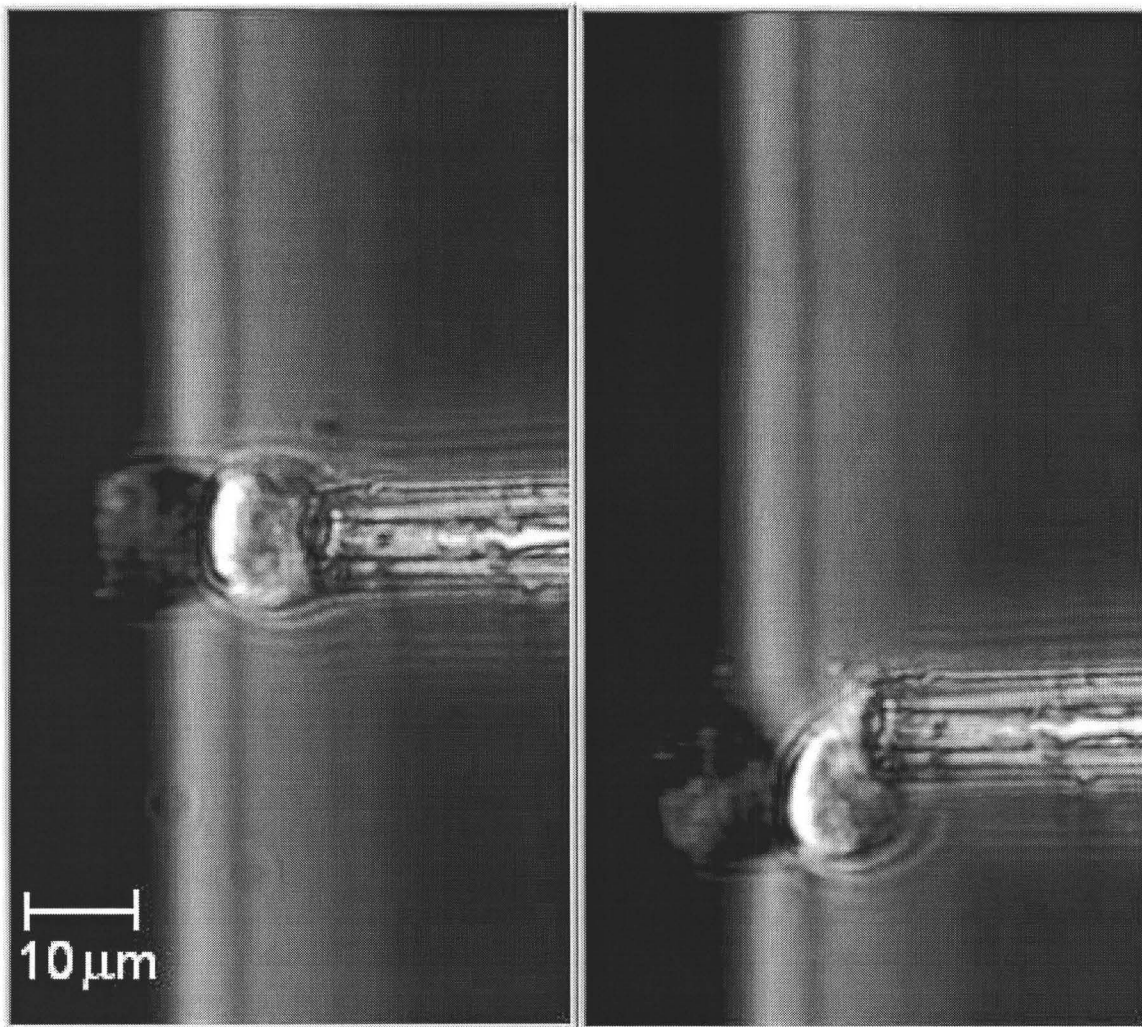

Figure 4.11: Phase-contrast images of HeLa cell being sheared by substrate coated with PLL.

The data for this experiment is shown in Fig. 4.12. The initial contact of 100 seconds was followed by a displacement of 100 μm at 0.1 μm/s as depicted in section (A). The substrate then waits another 100 seconds before moving 100 μm back to its original position and waits another 100 seconds (B). The substrate repeats the pattern in sections (C) and (D). When the substrate starts the last section however, the adhesion is strong enough to pull the pipette out of the field of view where the graph ends (E). As with the previous graph, the cantilever was not calibrated at the

time and as such we do not know the exact forces involved. However, the cantilevers made during this period had spring constants in the 2-5 nN/μm range and it is reasonable to assume a similar value for these cases. We can immediately see that the scale of forces involved in biological adhesion approaches the high nN range.

There are so many interesting things happening in Fig. 4.12 that it should come as no surprise that much experimental efforts were made to reproduce such data. Much of these efforts were concentrated on fabricating clean and uniform substrates, using different methods to coat the silicon with PLL. Immersing the substrate in PLL overnight, or letting a drop of the solution evaporate thereby ensuring the PLL was left on the surface. Different substrates were also tried, such as glass from a glass coverslip and polystyrene coated silicon, both with and without PLL. Slower velocities as low as 0.1 μm/s were also tried. Severe compression of the cell against the substrate was also attempted in order to try and promote adhesion but without any improvement. The length of contact before initial motion was also extended to 5-10 minutes in some cases, which often increased the initial strength of static friction but without any effect on subsequent adhesive behaviour. Unfortunately, the drastic behaviour seen in Fig. 4.12was only seen twice more during a year of experiments without any clue as to the reason behind it, besides the possibility that it was specific to those individual cells. Before leaving this chapter I will close with some remarks and speculation. Section (A) shows the cell sticking with a force which seems to oscillate in magnitude. When the substrate moves the other way (B), there is an initial stick followed by purely kinetic friction. This could be explained by the fact that when the substrate changes direction the cell rolls out of the pipette, presenting a different portion of its membrane to the surface. This new area could have been devoid of adhesion proteins as they may have diffused into the first contact area. When the substrate starts the third section of motion (C), the adhesion is even stronger and increases as time goes on. This indicates that the cell is actively adhering to the substrate, possibly by increasing the number of adhesion proteins in the contact area. During section (D), the cell again rolls onto the same side as in the second section. This time however, we have stick-slip motion which is increasing in magnitude, again pointing to receptor activity within the membrane. The last section (E) is cut short due to the adhesion being so strong that the cell and pipette are dragged out of the field of view. Overall, this graph illustrates the complex behaviour of the cell. Looking at each section individually however, we can begin to disinguish either periodic or monotonic trends to this behaviour. Finding a way to reproduce and control this behaviour is certainly a worthwhile scientific endeavour, especially since this type of measurement is what truly sets this new micropipette friction technique apart from typical adhesion experiments.
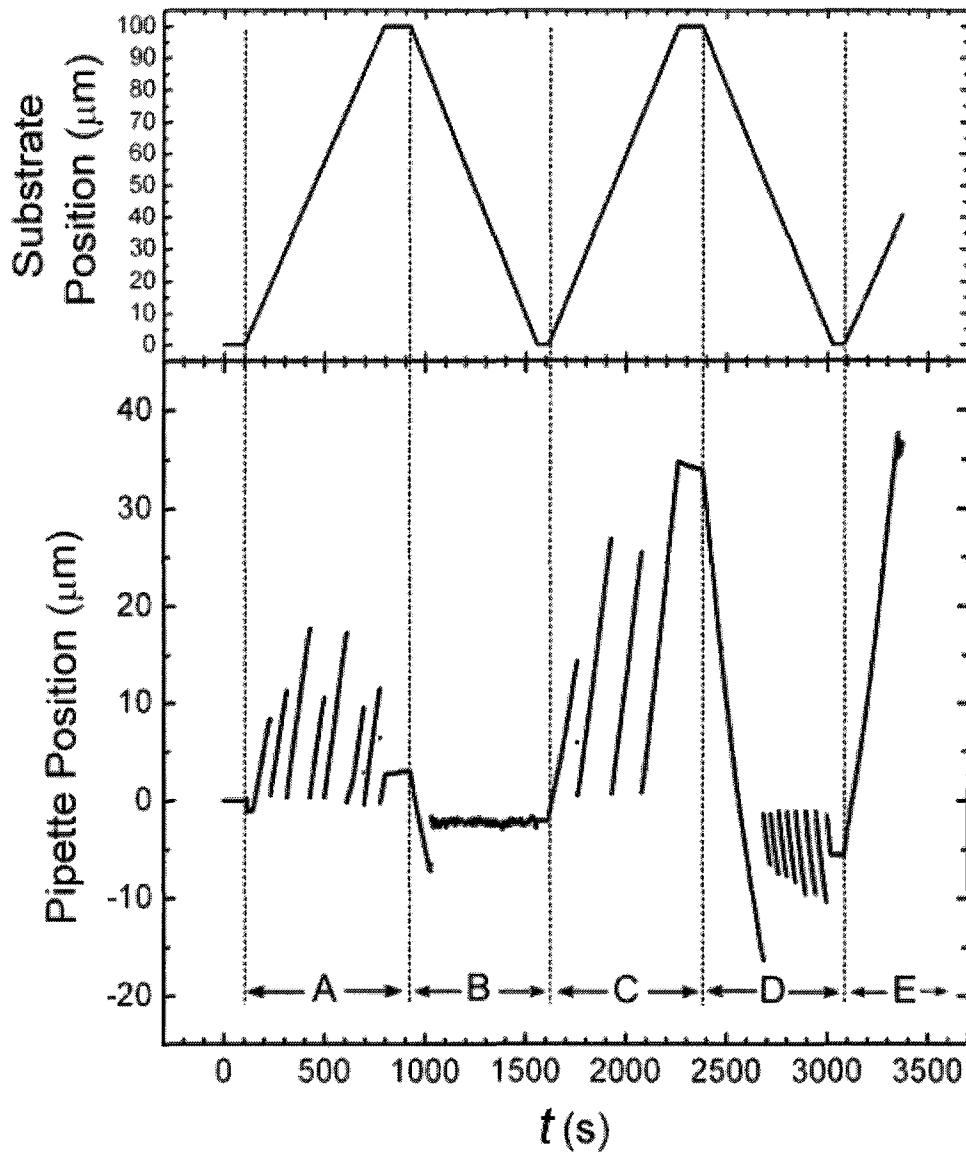
Figure 4.12: Vertical pipette position (friction force) as a function of time graph showing stick-slip motion of HeLa cell on PLL.

Chapter 5

Conclusions

The study of biological systems is one of the fastest growing fields of science in the world today. This accelerating rate of progress is in large part due to the advent of new analytical tools initially being invented for other disciplines such as physics. One of the main goals of this project has been to further develop the micropipette cantilever techniques started by Marie-Josée Colbert roughly 5 years ago. By adding the secondary cantilever to our instrument it has become possible to measure two forces simultaneously. Although this project has not delved very deeply into the details of biological adhesion, it has demonstrated the versatility of our techique. The custom-made micropipette cantilevers allow us to directly probe forces over five orders of magnitude, from 0.1 - 10000 nN. Our technique also allows us to observe the shear or compression deformation of the object throughout the entire experiment. While the non-invasive nature of the technique makes it especially suitable for studying living cells it can be applied to a wide range of other micron sized objects as shown by the colloidal studies.

With any new technique however there are always experimental obstacles to overcome. The majority of the results from the cell experiments lacked reproducibility. This was to be expected however, since each cell is both complex and unique, controlling the experimental parameters becomes quite difficult. This prompted us to simplify the experiment by studying polystyrene beads. The larger forces involved in the bead experiments made the results less prone to noise, leading to a very clear relationship between the normal and friction force as was expected.

Reproducibiliy aside, many of the measurements obtained corroborate the potential of this technique. The kinetic friction experiment on a HeLa cell produced very precise measurements of both the friction and normal force allowing us to calculate the coefficient of kinetic friction between the cell and silicon substrate. By varying the length of time for which the cell and substrate are at rest with respect to each other we were also able study the time dependence of the maximum force of static friction. These preliminary experiments indicate that the cells become more adhered to a PLL-coated substrate as time goes on, whereas the adhesion to a pure silicon substrate remains

relatively constant for the timescales being studied. This result signifies that the interaction between the cell and silicon may be purely colloidal whereas specific adhesion may be responsible for the time dependent forces between the cell and PLL. Studying this relation between time and adhesion strength is precisely the avenue we wished to explore in the first place.

Whether this micropipette technique is used to study the dynamics of bond formation, detachment, cell compression or shear, several refinements can be made. Reducing the plethora of possible adhesion molecules by blocking certain receptors on cells or using coated beads is definitely an important option to consider. Perhaps the easiest and most exciting improvement would be to replace the current chamber which houses the cells and media with a temperature controlled chamber. From a colloidal point of view, this would make it possible to study any entropic effects such as steric hindrance. From a biological point of view, it could be used to study the kinetics of bond formation or other cell functions. Adding piezo actuators to the substrate motion controllers could also make it possible to study the substrate/cell interaction in the nanometer range and access even slower lengthscales. Whatever the future holds for this nascent project it will likely evolve considerably in the coming years.

Appendix A

Appendix

A.1   Time dependence of adhesion for a HeLa cell on PLL

The cantilevers for all the examples in this appendix had spring constants in the 1-5 nN/μm range.
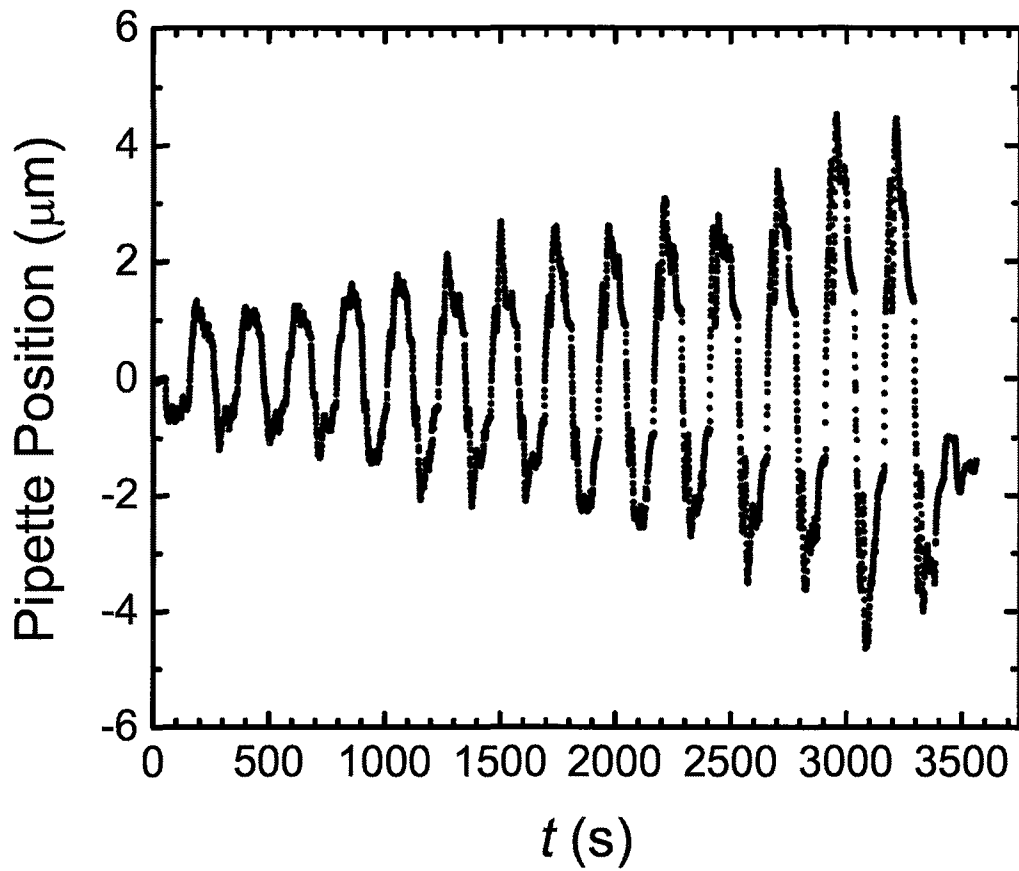
Figure A.1: Vertical pipette position (friction force) as a function of time for a HeLa cell on PLL with an initial wait time of $t=2$ s and an increase in wait time of 2 seconds every loop.

Figure A.2: Vertical pipette position (friction force) as a function of time for a HeLa cell on PLL with an initial wait time of t=2 s and an increase in wait time of 2 seconds every loop.
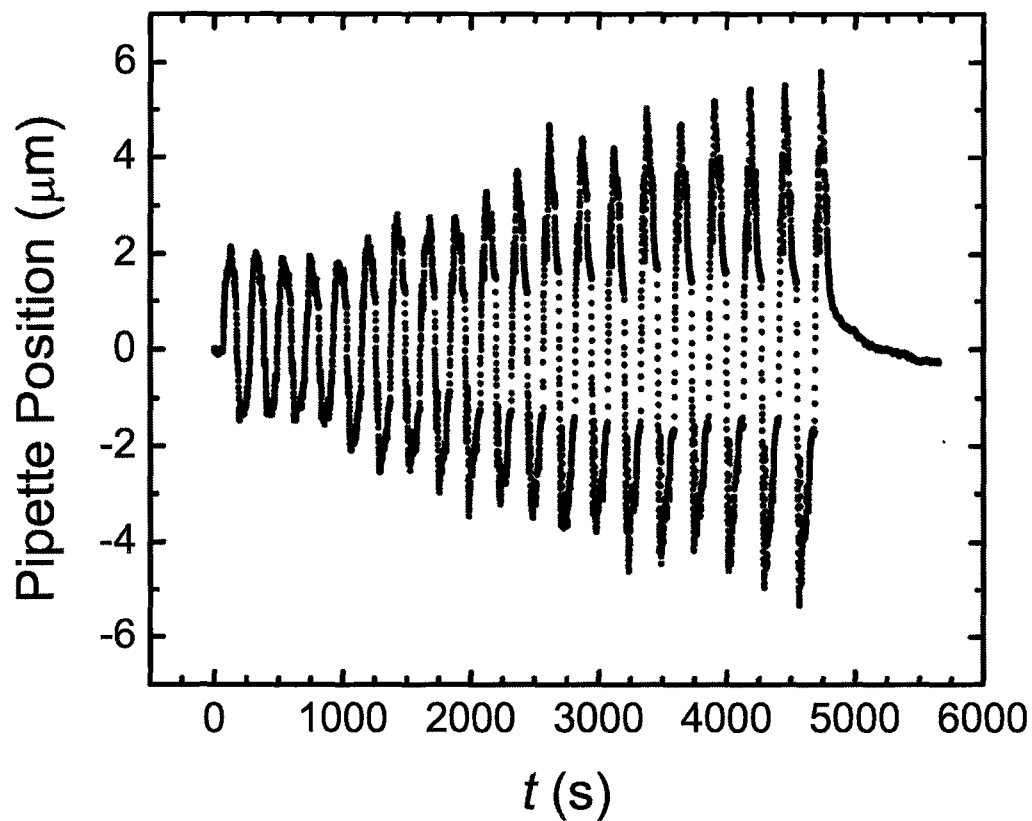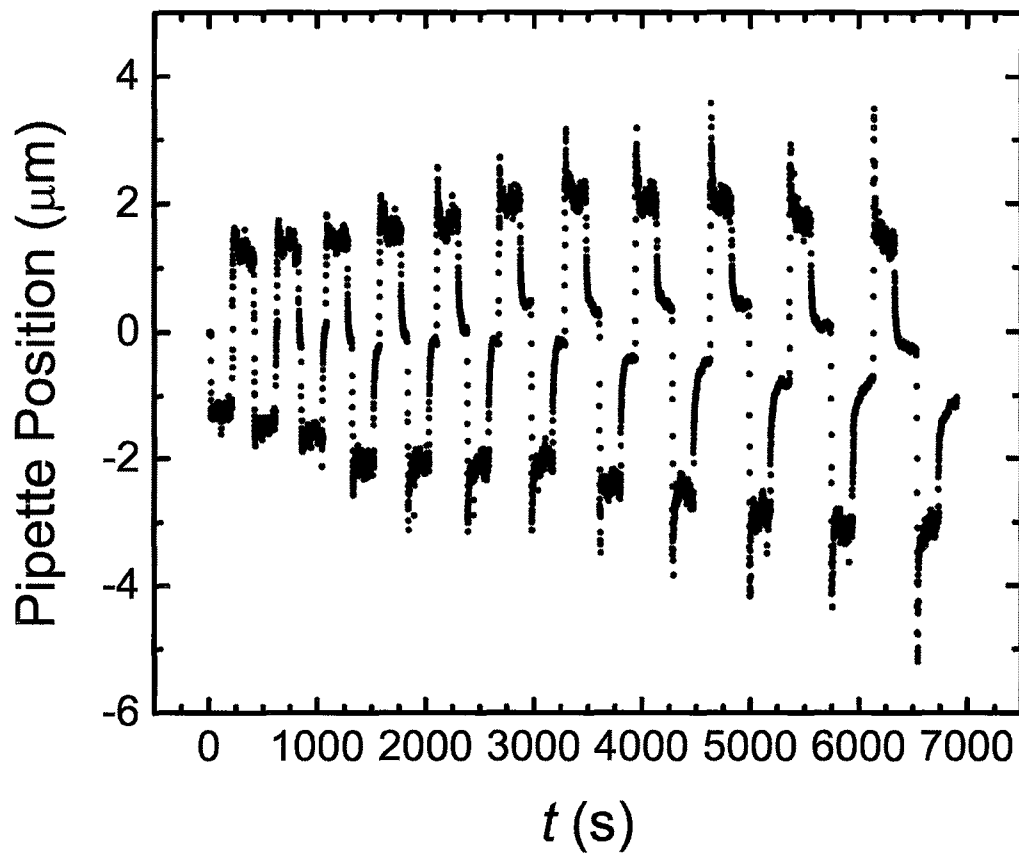
Figure A.3: Vertical pipette position (friction force) as a function of time for a HeLa cell on PLL with an initial wait time of $t=0$ s and an increase in wait time of 20 seconds every loop.

Bibliography

[1] Roger Kornu, William J. Maloney, Michael A. Kelly, and R. Lane Smith. Osteoblast adhesion to orthopaedic implant alloys: Effects of cell adhesion molecules and diamond-like carbon coating. *Journal of Orthopaedic Research*, 14:871–877, 1996.

[2] R.A.L. Jones. *Soft Condensed Matter*. Oxford University Press, New York, 2002.

[3] D. Boal. *Mechanics of the cell*. Cambridge University Press, Cambridge, 2002.

[4] Jacob Israelachvili. *Intermolecular & Surface Forces*. Academic Press, San Diego, 1991.

[5] Harvey Lodish, Arnold Berk, S. Lawrence Zipursky, Paul Matsudaira, David Baltimore, and James Darnell. *Molecular Cell Biology*. W.H. Freeman and Company, New York, 2000.

[6] E.A. Evans. Physical actions in biological adhesion. *Handbook of Biological Physics*, 1:723–753, 1995.

[7] G. Weber. Energetics of ligand binding to proteins. *Adv. Prot. Chem.*, 29:1–83, 1975.

[8] N.M. Green. Avidin. *Adv. Prot. Chem.*, 29:85–133, 1975.

[9] E.A. Evans, D. Berk, and A. Leung. Detachment of agglutinin-bonded red blood cells. *Biophysical Journal*, 59:838–848, 1991.

[10] E.A. Evans, D. Berk, and A. Leung. Detachment of agglutinin-bonded red blood cells. *Biophysical Journal*, 59:849–860, 1991.

[11] E.A. Evans and K. Ritchie. Dynamic strength of molecular adhesion bonds. *Biophysical Journal*, 72(4):1541–1555, 1997.

[12] R. Merkel, P. Nassoy, A. Leung, K. Ritchie, and E. Evans. Energy landscapes of receptor ligand bonds explored with dynamic force spectroscopy. *Nature*, 397(6714):50–53, 1999.

[13] E.A. Evans. Minimum energy analysis of membrane deformation applied to pipet aspiration and surface adhesion of red blood cells. *Biophysical Journal*, 30:265–284, 1980.

[14] E.A. Evans, K. Ritchie, and R. Merkel. Sensitive force technique to probe molecular adhesion and structural linkages at biological interfaces. *Biophysical Journal*, 68:2580–2587, 1995.

[15] E. Decave, Y. Garrivier, D. Brechet, F. Bruckert, and B. Fourcade. Peeling process in living cell movement under shear flow. *Phys. Rev. Lett.*, 89(10):108101–01, 2002.

[16] E. Decave, Y. Garrivier, D. Brechet, F. Bruckert, and B. Fourcade. Shear flow-induced detachment kinetics of dictyostelium discoideum cells from solid substrate. *Biophysical Journal*, 82(5):2383–2395, 2002.

[17] D. Garrivier, E. Decave, Y. Brechet, F. Bruckert, and B. Fourcade. Peeling model for cell detachment. *Eur. Phys. J. E*, 8:79–97, 2002.

[18] R. Cotterill. *Biophysics: An introduction.* John Wiley & Sons, Ltd, Chichester, 2002.

[19] D.J. Goetz, M.E. el Sabban, B.U. Pauli, and Hammer D.A. Dynamics of neutrophil rolling over stimulated endothelium in vitro. *Biophysical Journal*, 66:2202–2209, 1994.

[20] A. Yamamoto, S. Mishima, N. Maruyama, and M. Sumita. Quantitative evaluation of cell attachment to glass, polystyrene, and fibronectin- or collagen-coated polystyrene by measurement of cell adhesive shear force and cell detachment energy. *Journal of Biomedical Materials Research*, 50(2):114–124, 2000.

[21] A. Yamamoto, S. Mishima, N. Maruyama, and M. Sumita. A new technique for direct measurement of the shear force necessary to detach a cell from a material. *Biomaterials*, 19(7-9):871–879, 1998.

[22] E.L. Florin, V.T. Moy, and H.E. Gaub. Adhesion forces between individual ligand-receptor pairs. *Science*, 264(5157):415–417, 1994.

[23] G.W. Francis, L.R. Fisher, R.A. Gamble, and D. Gingell. Direct measurement of cell detachment force on single cells using a new electromechanical method. *Journal of cell science*, 87:519–523, 1987.

[24] Hugh D. Young and Roger A. Freedman. *University Physics.* Addison-Wesley, Reading, 1996.

[25] B.N.J. Persson. *Sliding Friction: Physical Principles and Applications.* Springer-Verlag, Berlin, 2000.

[26] C. Drummond and J. Israelachvili. Dynamic phase transitions in confined lubricant fluids under shear. *Phys. Rev. E*, 2:SA89–SA98, 2001.

[27] J. Israelachvili, P. McGuiggan, M. Gee, A. Homola, A. Robbins, and P. Thompson. Liquid dynamics in molecularly thin films. *J. Phys. Condensed Matter*, 63(4):041506–1, 1990.

[28] T. Baumberger, C. Caroli, and O. Ronsin. Self-healing slip pulses and the friction of gelatin gels. *Eur. Phys. J. E*, 11(1):85–93, 2003.

[29] T. Baumberger, C. Caroli, and O. Ronsin. Dynamic phase transitions in confined lubricant fluids under shear. *Phys. Rev. Lett.*, 88(7):075509–1, 2002.

[30] U. Raviv, S. Giasson, N. Kampf, J. Gohy, R. Jerome, and J. Klein. Lubrication by charged polymers. *Nature*, 425(6954):163–165, 2003.

[31] B.N.J. Persson, U. Tartaglino, O. Albohr, and E. Tosatti. Rubber friction on wet and dry road surfaces: The sealing effect. *Phys. Rev. B*, 71:035428, 2005.

[32] D. Mazia, G. Schatten, and W. Sale. Adhesion of cells to surfaces coated with polylysine. *Journal of Cell Biology*, 66:198–200, 1975.